Probing the holographic model of $\mathcal{N} = 4$ SYM rotating quark-gluon plasma

Anastasia Golubtsova[1,2,*] and Nikita Tsegelnik[1,†]

[1]*Bogoliubov Laboratory of Theoretical Physics, JINR, Joliot-Curie str. 6, Dubna 141980, Russia*
[2]*Steklov Mathematical Institute, Russian Academy of Sciences, Gubkina str. 8, Moscow 119991, Russia*

(Received 6 April 2023; accepted 8 May 2023; published 30 May 2023)

We study Wilson loops in holographic duals of the $\mathcal{N} = 4$ SYM quark-gluon plasma. For this we consider the Schwarzschild-AdS$_5$ and Kerr-AdS$_5$ black holes, which are dual to the nonrotating and rotating quark-gluon plasmas, correspondingly. From temporal Wilson loops we find the heavy quark potentials in both backgrounds. For the temperature above the critical one we observe the Coulomb-like behavior of the potentials. We find that increasing the rotation the interquark distance decreases, we also see that the increase of the temperature yields the similar behavior. Moreover, at high temperatures values of the potentials in Kerr-AdS$_5$ are close to that one calculated in the Schwarzschild-AdS$_5$ black hole. We also explore holographic lightlike Wilson loops from which the jet-quenching parameters of a fast parton propagating in the QGP are extracted. We find that the rotation increases the value of the jet-quenching parameter. However, at high temperatures the jet-quenching parameters have a cubic dependence on the temperature as for the AdS black brane.

DOI: 10.1103/PhysRevD.107.106017

I. INTRODUCTION

Recently, much interest has been paid to study and understand a rotating quark-gluon plasma (QGP). It can be created in noncentral heavy-ion collisions, where large initial orbital momentum of ions is partially transferred to the created medium, that leads to the relativistic rotation [1,2]. The spacetime structure of the vorticity field, which also arises in noncentral heavy-ion collisions, may have nontrivial geometrical features, like femto-vortex sheets [3] or elliptic vortex rings [4,5]. The nonzero vorticity may result in different effects, for instance, the chiral vortical effect (for a review, see [6]). Unfortunately, there is no direct way to investigate the QGP, so different probes are used to extract the information about the plasma properties.

One of these probes is the global polarization of Λ-hyperons. Being produced in a rotating medium, particles with spin obtain a polarization that depends on the magnitude of rotation [7,8]. In fact, by virtue of the $\mathcal{P}$-violation in the weak decay $\Lambda \to \mathrm{p} + \pi$, the angular distribution of the detected protons depends on the orientation of the Λ's spin. In other words, measuring the proton distributions and restoring the polarization of the Λ-hyperons, it is possible to estimate the magnitude of the QGP rotation. This experiment was carried out by the STAR Collaboration [9,10]. Surprisingly, the extracted averaged vorticity value is $\omega \approx 10^{22}$ s^{-1}, which leads to the hypothesis that QGP is the fastest rotating fluid ever observed in nature [10,11].

In a series of experiments [12–15] it was found that hadron spectra with high transverse momenta p_{T} are suppressed in the medium. The suppression of elliptical flows v_2 was also observed. This may indicate that the medium formed in heavy-ion collisions is dense and nontransparent. The increase of the nuclear modification factor R_{AA}, which observed at experiments, also predicts that the QGP is an opaque fluid.

Since the experiments also indicate that the quark-gluon plasma produced in HIC is a strongly-coupled fluid [12], it is quite reasonable to examine this system in the framework of the holographic duality [16–18]. In this approach the object of study is replaced by $\mathcal{N} = 4$ SYM plasma, that is much more simpler and provides a qualitative insights of the strongly-coupled regime. It worth to be noted that at finite temperature strongly-coupled $\mathcal{N} = 4$ SYM and QCD above the deconfinement temperature have much in common. At high temperature lattice simulations show that the stress tensor becomes traceless, which may indicate a conformal symmetry [19].

Note that $\mathcal{N} = 4$ SYM defined on $R \times \mathbb{R}^3$ at zero temperature does not have a confinement-deconfinement phase transition. The holographic calculations in backgrounds with flat boundaries also predict that there is no confinement-deconfinement phase transition in the dual

*golubtsova@theor.jinr.ru
†tsegelnik@theor.jinr.ru

theory on $R \times \mathbb{R}^3$ [20–24]. However, the situation changes if one discusses $\mathcal{N} = 4$ SYM on $R \times \mathbb{S}^3$. In [25] it was shown that a first-order phase transition occurs in the free $\mathcal{N} = 4$ SYM on $R \times \mathbb{S}^3$ at the Hagedorn temperature, in [26] it was discussed for the one-loop order in the weak-coupling expansion. Moreover, using the integrability the Hagedorn temperature was calculated at any value of the 't Hooft coupling in [27].

From the holographic point of view the strongly-coupled $\mathcal{N} = 4$ SYM on $R \times \mathbb{S}^3$ at finite temperature is dual to a 5D AdS black hole with a conformal boundary $R \times \mathbb{S}^3$, i.e., a spherical horizon. In turn, a 5D AdS black hole with a conformal boundary $R \times \mathbb{S}^3$ has the first order Hawking-Page phase transition, which according to the holographic dictionary corresponds to the deconfinement phase transition in dual theory [28,29]. Thus, the quark-gluon plasma state at equilibrium can be associated to the AdS black hole with a larger radius.

Following the holographic dictionary, a rotating AdS black hole with a spherical horizon is a gravitational dual to the rotating $\mathcal{N} = 4$ SYM plasma [30–33]. Like Schwarzschild-AdS black holes, rotating AdS black holes also have a Hawking-Page phase transition [34–36], which corresponds to a phase transition in the dual theory. Note that the phase transition in Kerr-AdS$_5$ happens for certain values of the rotational parameters. If at least one of the rotational parameters is large enough then the phase transition disappears [37]. The calculations of the critical temperature T_c in the Kerr-AdS$_5$ background predict that T_c decreases with the rotation [37]. This is also observed in other holographic backgrounds for studies of the rotating quark-gluon plasma [38,39] and effective models [40–42]. However, it was shown in lattice calculations [43,44] that rotating gluons increase the critical temperature, while the rotating fermions decrease it.

In work [45] it was discussed holographic off-center heavy-ion collisions using the 5D Kerr-AdS black hole with two nonzero rotational parameters. In [46] the authors extracted analytic expressions for transport coefficients (the shear viscosity, the longitudinal momentum diffusion coefficient, etc.) and calculated quasinormal modes for spinning black holes. Scalar perturbations of the Kerr-AdS$_5$ background with generic rotational parameters were also calculated in [47], where it was shown that quasinormal modes in Kerr-AdS$_5$ at low temperature can be encoded by zeros of the Painleve V tau function. In [48] circular pulsating string solutions in the 5D Kerr-AdS black hole with equal rotational parameters were found.

Recently, within the framework of the holographic duality the energy loss of heavy quarks were explored in the rotating quark-gluon plasma in [37,49,50]. In these works a holographic description of a rotating QGP is given by a 5D Kerr-AdS black hole, while the heavy quarks at finite temperature are associated by endpoints of open strings in the AdS black hole. The endpoints are located on the conformal boundary of the black hole background, so the string hanging down to the black hole horizon. In [38,39,51] thermodynamic quantities, Polyakov and Wilson loops in a holographic rotating background were studied, which mimic results for lattice simulations for a pure gluon rotating system and a rotating system with $N = 2$ flavors.

In this paper we probe $\mathcal{N} = 4$ SYM quark-gluon plasma on $R \times \mathbb{S}^3$ by Wilson loops using holography. The dual description of the expectation value of the rectangular Wilson loop can be done in terms of the minimized Nambu-Goto action of a classical string, where both endpoints attach to the conformal boundary of the AdS black hole, while the string stretches down to the horizon [22,23]. In this work we focus on temporal and lightlike Wilson loops. From the expectation value of a temporal Wilson loop we extract a heavy quark-antiquark potential and explore the affect of the rotation on it.

The lightlike Wilson loops can be used to study the jet-quenching phenomenon in the quark-gluon plasma, which is of interest since high-energy particles propagating through the QGP are strongly decelerated [52,53]. Following [54,55], the so-called jet-quenching parameter $\hat{q}$ is defined as a coefficient of the L^2 term in the logarithm of a long lightlike Wilson loop of width L. It encodes the description of energy losses for relativistic partons moving in the quark-gluon plasma. More precisely, the parameter $\hat{q}$ gives the squared average transverse momentum exchange between the medium and highly-energetic parton per unit path length. In [56] the holographic calculations for the jet-quenching parameter were generalized for the case of an arbitrary diagonal metric. Using holographic models, a modification of an ensemble of jets was analyzed in [57,58], which propagate through a strongly-coupled plasma. Thus, using the AdS/CFT correspondence we are also able to find and analyze the jet-quenching parameter. The holographic computations in the planar AdS black brane background yield the following relation [54,55]:

$$\hat{q} = \frac{\pi^{3/2}\Gamma\left(\frac{3}{4}\right)}{\Gamma\left(\frac{5}{4}\right)}\sqrt{\lambda}T^3. \tag{1.1}$$

It is worth noting that the jet-quenching parameter $\hat{q}$ in (1.1) is not proportional to the "number of scattering centers", which is $\propto N_c^2$. Moreover, the value of $\hat{q}$ in QCD is smaller than that one predicted by (1.1).

In this work we show that the jet-quenching parameters in the Schwarzschild-AdS$_5$ and the Kerr-AdS$_5$ at high temperatures have the same dependence on T as for the AdS black brane (1.1). We also find that rotation increases the values of $\hat{q}$.

The paper is organized as follows. In Sec. II we start with a review of the Schwarzschild-AdS$_5$ and Kerr-AdS$_5$ black hole solutions. Then we briefly discuss the calculation of

rectangular Wilson loops in holography. In Sec. III we calculate the expectation values of temporal Wilson loops in the Schwarzschild-AdS$_5$ and Kerr-AdS$_5$ black hole backgrounds and then analyze the corresponding quark-antiquark potentials. In Sec. IV we evaluate lightlike Wilson loops and estimate the jet-quenching parameters in the Schwarzschild-AdS$_5$ and Kerr-AdS$_5$ black holes. In Sec. V we conclude and give a discussion.

II. SETUP

A. Gravity backgrounds

We consider a five-dimensional gravity theory with a negative cosmological constant Λ

$$S=\frac{1}{2\kappa^2}\int d^5x\sqrt{-g}(R_5-2\Lambda). \tag{2.1}$$

The Einstein equations following from (2.1) are

$$R_{\mu\nu}=\frac{\Lambda}{3}g_{\mu\nu}, \tag{2.2}$$

where we suppose $\Lambda=-6/\ell^2$. The simplest black hole solution of a mass M and a spherical horizon to Eq. (2.2) is the Schwarzschild-AdS$_5$ black hole with the metric

$$\begin{aligned}ds^2=&-\frac{f(r)}{r^2}\mathrm{d}t^2+\frac{r^2}{f(r)}\mathrm{d}r^2\\&+r^2(\mathrm{d}\theta^2+\sin^2\theta\mathrm{d}\phi^2+\cos^2\theta\mathrm{d}\psi^2),\end{aligned} \tag{2.3}$$

where the function $f(r)$ is

$$f(r)=r^2+\ell^{-2}r^4-2M. \tag{2.4}$$

In (2.3) the angular coordinates are defined as $0\le\theta\le\pi/2$, $0\le\phi,\psi\le2\pi$. It is worth noting, that the horizon of the black hole is defined as a greater root of the equation $f(r)/r^2=0$, thus we have

$$r_h=\frac{\ell\sqrt{\sqrt{8\ell^{-2}M+1}-1}}{\sqrt{2}}. \tag{2.5}$$

The Hawking temperature of the black hole (2.3) is given by

$$T_{\mathrm{H}}=\frac{2r_h^2+\ell^2}{2\pi r_h\ell^2}. \tag{2.6}$$

Another black hole solution with a spherical horizon to Eq. (2.2) is the Kerr-AdS$_5$ black hole with arbitrary rotational parameters a and b (in the static-at-infinity frame [36])

$$\begin{aligned}ds^2\simeq&-(1+y^2\ell^{-2})\mathrm{d}T^2+\frac{\mathrm{d}y^2}{1+y^2\ell^{-2}-\frac{2M}{\Delta^2y^2}}+\frac{2M}{\Delta^3y^2}\\&\times(\mathrm{d}T-a\sin^2\Theta\mathrm{d}\Phi-b\cos^2\Theta\mathrm{d}\Psi)^2\\&+y^2(\mathrm{d}\Theta^2+\sin^2\Theta\mathrm{d}\Phi^2+\cos^2\Theta\mathrm{d}\Psi^2),\end{aligned} \tag{2.7}$$

with

$$\Delta=1-a^2\ell^{-2}\sin^2\Theta-b^2\ell^{-2}\cos^2\Theta. \tag{2.8}$$

In (2.7)–(2.8) the angular coordinates run as for the Schwarzschild-AdS$_5$; $0\le\Theta\le\frac{\pi}{2}$, $0\le\Phi,\Psi\le2\pi$. The horizon y_+ of the Kerr-AdS$_5$ black hole is a greater root of the equation

$$1+y^2\ell^{-2}-\frac{2M}{\Delta^3y^2}=0. \tag{2.9}$$

Correspondingly, the Hawking temperature reads

$$T_{\mathrm{H}}=\frac{1}{2\pi}\left(y_+(1+y_+^2\ell^{-2})\left(\frac{1}{y_+^2+a^2}+\frac{1}{y_+^2+b^2}\right)-\frac{1}{y_+}\right). \tag{2.10}$$

It is easy to see, that for $a=b=0$ the Kerr-AdS$_5$ metric (2.7) comes to the Schwarzschild-AdS$_5$ (2.3) background, i.e., $y_+|_{a=b=0}=r_h$.

The dependence of the Hawking temperature on y_+/ℓ (r_h/ℓ) is shown in Fig. 1. The rotational parameters belong to the range $0\le a,b\le\ell$, so it is useful to take a fraction of ℓ as a value of a or b. We see that both the Schwarzschild-AdS$_5$ and Kerr-AdS$_5$ black holes have minima of the Hawking temperature $T_{\mathrm{H}}^{\min}$. In the case of the Schwarzschild-AdS$_5$ black hole $T_{\mathrm{H}}^{\min}$ is defined by

$$T_{\mathrm{H}}^{\min}=\frac{\sqrt{2}}{\pi\ell},\quad\text{with}\quad r_h=\frac{\ell}{\sqrt{2}}. \tag{2.11}$$

Note that the black hole solution does not exist for $T<T_{\mathrm{H}}^{\min}$. In our calculations we set $\ell=0.55$ fm, so $T_{\mathrm{H}}^{\min}\approx0.16$ GeV. Above this point, there are two possible values of the temperature, corresponding to the small ($r_h<\ell/\sqrt{2}$) and big ($r_h>\ell/\sqrt{2}$) black holes, but only the latter is allowed as a stable equilibrium [29]. The Hawking-Page phase transition occurs at the temperature $T_c\ge3/(2\pi\ell)\approx0.17$ GeV. Following the holographic dictionary the Hawking-Page phase transition corresponds to the confinement-deconfinement phase transition [28].

For the Kerr-AdS$_5$ black hole the Hawking-Page phase transition also takes place. However, the presence of rotation changes the behavior of the temperature; below some critical values of the rotational parameters the temperature is three-valued function on y_+. From the other hand, a stronger rotation leads to the absence of the

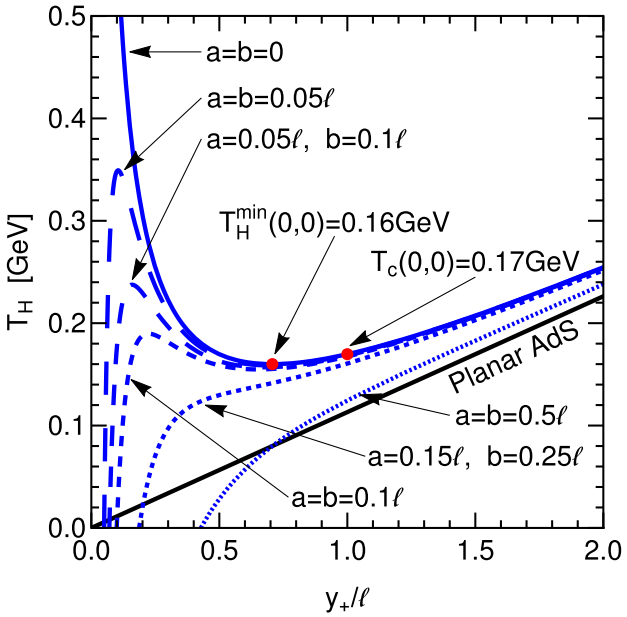

FIG. 1. The Hawking temperature T_{H} as a function of y_+/ℓ (r_h/ℓ). The case of the Schwarzschild-AdS$_5$ black hole ($a = b = 0$) is shown by a blue solid curve, the Hawking temperatures for the Kerr-AdS$_5$ background for various values of the rotational parameters are shown by dashed curves from top to bottom according to increasing values of a and b. The Hawking temperature for the AdS black hole with planar horizon is depicted by the black solid line.

temperature ambiguity, and, hence, the Hawking-Page phase transition disappears [37].

In Fig. 1 we also compare the Hawking temperatures of the 5D AdS black holes with planar and spherical horizons. We see that for the same values of the horizons, T_{H} of the black hole with spherical symmetry has a greater value than that one for the planar AdS$_5$ black hole. The spherical AdS black hole with a large horizon, corresponding a high temperature, behaves similar to the planar AdS black holes.

Note that the conformal boundary for both solutions (2.3), (2.7) is defined at infinity of the holographic coordinates $r \to +\infty$ ($y \to +\infty$) and has the form[1]

$$ds^2 = -\mathrm{d}t^2 + \mathrm{d}\theta^2 + \sin^2\theta \mathrm{d}\phi^2 + \cos^2\theta \mathrm{d}\psi^2. \tag{2.12}$$

B. Wilson loops in holography

Following the holographic prescription the expectation value of the Wilson loop on the contour $\mathcal{C}$ can be calculated using a Nambu-Goto action of an open string in a holographic background [20,21]

$$\langle W(\mathcal{C})\rangle = e^{-S_{\mathrm{NG}}}, \tag{2.13}$$

where S_{NG} is a regularized action of the string. Hence, consider a string which is governed by the Nambu-Goto action

$$S_{\mathrm{NG}} = \frac{1}{2\pi\alpha'}\int \mathrm{d}\sigma\mathrm{d}\tau\sqrt{-\det(g_{\alpha\beta})}, \tag{2.14}$$

where σ and τ parametrized the string world sheet, $(g_{\alpha\beta})$ is the induced metric on the worldsheet

$$g_{\alpha\beta} = G_{MN}\partial_\alpha X^M \partial_\beta X^N, \tag{2.15}$$

G_{MN} is a spacetime metric, X^M are embedding coordinates, and α, β are world sheet indices. To consider a temporal recangular Wilson loop, one should take one temporal and one spacial coordinate to parametrize the string world sheet.

It's known that the interquark potential is related to the expectation value of the static temporal Wilson loop as follows:

$$\langle W(\mathcal{C})\rangle \sim e^{-\mathcal{T}V(L)}, \tag{2.16}$$

where the distance between quarks L and the temporal extent of the Wilson loop $\mathcal{T} \to \infty$. Thus, taking into account (2.13) the quark-antiquark potential can be found in the following way

$$V_{q\bar{q}} = \left.\frac{S_{\mathrm{NG}}}{\mathcal{T}}\right|_{\mathcal{T}\to\infty}. \tag{2.17}$$

A generalization to the finite-temperature case was suggested in [22,23]. In the work [24] the quark-antiquark potential was explored in the rotating D3-brane background.

Note that the Cornell potential [59,60] includes the Coulomb term, which dominates at short distances, and the linear-confining term

$$V_{q\bar{q}} = \sigma L - \frac{\kappa}{L}, \tag{2.18}$$

where L is the interquark distance, κ and σ are the Coulomb strength and string tension parameters, respectively. In the confined phase the expectation value of the Wilson loop reproduces an area law

$$\langle W(\mathcal{C})\rangle \sim e^{-\sigma LT} = e^{-\sigma \mathrm{Area}(\mathcal{C})}. \tag{2.19}$$

Using the expectation value of the lightlike Wilson loop on the contour $\mathcal{C}$ in the adjoint representation one is able to find the jet-quenching parameter $\hat{q}$ for a fast parton [54,55]

$$\langle W^A(\mathcal{C})\rangle \approx \exp\left[-\frac{1}{4\sqrt{2}}\hat{q}L^- L^2\right], \tag{2.20}$$

where L^- is a large side of the rectangular contour $\mathcal{C}$ and L is a short side. At the same time, the Wilson-loop operator

[1]For the Kerr-AdS$_5$ the coordinates in (2.12) should be capital.

in the adjoint representation is related to the Wilson-loop operator in the fundamental representation as follows:

$$\langle W^A(\mathcal{C})\rangle \approx \langle W^F(\mathcal{C})\rangle^2. \tag{2.21}$$

Following the holographic dictionary (2.13), we have

$$\langle W^F(\mathcal{C})\rangle = e^{-S_{\rm NG}}. \tag{2.22}$$

Taking (2.20) into account we find the relation for the jet-quenching parameter

$$\hat{q} = \frac{4\sqrt{2}}{L^- L^2} S_{\rm NG}. \tag{2.23}$$

III. HOLOGRAPHIC WILSON LOOPS

A. Wilson loop in Schwarzschild-AdS$_5$ black hole

It is instructive to start with a nonrotating case of the holographic background, so, first, we consider a holographic Wilson loop in the 5D Schwarzschild-AdS black hole with a spherical horizon (2.3)–(2.4).

Parametrizing the world sheet of the static string in the following way:

$$\tau = t, \qquad \sigma = \phi, \qquad \phi \in [0, 2\pi L_\Phi], \qquad r = r(\phi), \tag{3.1}$$

we get nonzero components of the induced metric (2.15)

$$\begin{aligned} g_{\tau\tau} &= G_{tt} = -\frac{f(r)}{r^2}, \\ g_{\sigma\sigma} &= G_{\phi\phi} + r'^2 G_{rr} = r^2\left(\sin^2\theta + \frac{r'^2}{f(r)}\right), \end{aligned} \tag{3.2}$$

where $f(r)$ is defined by (2.4) and we denoted $r' \equiv {\rm d}r/{\rm d}\phi$. The boundary conditions for the string endpoints are given by

$$r\left(\phi = -\frac{L_\phi}{2}\right) = r\left(\phi = \frac{L_\phi}{2}\right) = \infty. \tag{3.3}$$

In Fig. 2 we show the string configuration for (3.1) and (3.3).

Equations (3.1)–(3.3) yield the following expression for the Nambu-Goto action (2.14) of the string in the Schwarzschild-AdS$_5$ background

$$S = \frac{T}{2\pi\alpha'}\int_{-\frac{L_\phi}{2}}^{\frac{L_\phi}{2}} d\phi \sqrt{f(r)\sin^2\theta + r'^2}. \tag{3.4}$$

From (3.4) it is easy to find the integral of motion

$$\mathcal{H} = -\frac{\sin^2\theta\sqrt{f(r)}}{\sqrt{\sin^2\theta + \frac{r'^2}{f(r)}}} = -\frac{\ell}{C}. \tag{3.5}$$

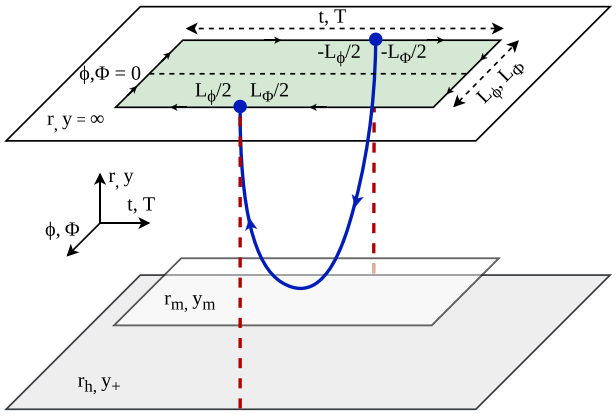

FIG. 2. The schematic illustration of the holographic Wilson loop configuration. The string endpoints are located at $\phi = \pm\frac{L_\phi}{2}$. The red dashed lines depict the configuration of the free quarks.

The string has a turning point, which is defined by $r'|_{\phi_m} = 0$, thus from (3.5) we have

$$-\frac{\sin^2\theta\sqrt{f(r)}}{\sqrt{\sin^2\theta + \frac{r'^2}{f(r)}}} = -\frac{\ell}{C}, \tag{3.6}$$

so the constant of integration is defined by

$$C = \left.\frac{\ell}{\sin\theta\sqrt{f(r)}}\right|_{r=r_m} \tag{3.7}$$

with $r_m = r(\phi_m)$. Note that r_m is located above the horizon r_h, see Fig. 2.

From Eq. (3.5) we find the equation of motion represented as

$$r'^2 = \sin^2\theta f(r)\left(\frac{C^2\sin^2\theta f(r)}{\ell^2} - 1\right). \tag{3.8}$$

Plugging (3.8) into the Nambu-Goto action (3.4) and coming to the integration in terms of r, we obtain

$$S_{\rm NG} = \frac{T}{\pi\alpha'}\int_{r_m}^{\infty} dr \frac{C\sin\theta\sqrt{f(r)}}{\sqrt{C^2\sin^2\theta f(r) - \ell^2}}. \tag{3.9}$$

From the other hand, we have the expression for the distance between quarks L_ϕ from (3.8),

$$\frac{L_\phi}{2} = \frac{\ell}{\sin\theta}\int_{r_m}^{\infty} dr \frac{1}{\sqrt{f(r)}\sqrt{C^2\sin^2\theta f(r) - \ell^2}}. \tag{3.10}$$

It worth to be noted that Eq. (3.9) has a divergence at the conformal boundary $r \to +\infty$ of the spacetime (2.3) and we have to regularize (3.9). The renormalization procedure represents a subtraction of the "self-energy" of two free static quarks, which holographically corresponds to the

action of the static straight strings stretched from the boundary $r=\infty$ to the horizon r_h,

$$S_0=\frac{T}{\pi\alpha'}\int_{r_h}^{\infty}dr\sqrt{-G_{tt}G_{rr}}=\frac{T}{\pi\alpha'}\left(\int_{r_m}^{\infty}dr+r_m-r_h\right). \tag{3.11}$$

Then, taking into account (3.11), the regularized action takes the form

$$\begin{aligned}S_{\rm NG}^{\rm ren}&=S_{\rm NG}-S_0\\&=\frac{T}{\pi\alpha'}\left(\int_{r_m}^{\infty}dr\left(\frac{C\sin\theta\sqrt{f(r)}}{\sqrt{C^2\sin^2\theta f(r)-\ell^2}}-1\right)-r_m+r_h\right).\end{aligned} \tag{3.12}$$

One can try to estimate the relation between $S_{\rm NG}^{\rm ren}$ (3.12) and L_ϕ (3.10). In order to find this we introduce the following notation in Eqs. (3.10) and (3.12)

$$S_{\rm NG}^{\rm ren}=\frac{T}{\pi\alpha'}I_1(r_m,C),\qquad L_\phi=2I_2(r_m,C). \tag{3.13}$$

The derivatives of these quantities with respect to C are related in the following way

$$\frac{\partial I_2(r_m,C)}{\partial C}=\frac{C}{\ell}\frac{\partial I_1(r_m,C)}{\partial C}. \tag{3.14}$$

Integrating lhs of Eq. (3.14), we obtain

$$\int_0^C\frac{\partial I_2(r_m,C)}{\partial C}dC=\frac{L_\phi}{2}+\frac{i}{\sin\theta}\int_{r_m}^{\infty}\frac{dr}{\sqrt{f(r)}}, \tag{3.15}$$

at the same time using integration by parts of rhs (3.14) one has

$$\int_0^C\frac{C}{\ell}\frac{\partial I_1(r_m,C)}{\partial C}dC=\frac{C}{\ell}\frac{\pi\alpha'}{T}S_{\rm NG}^{\rm reg}-\frac{1}{\ell}\int_0^C I_1(r_m,C)dC, \tag{3.16}$$

where we define

$$\begin{aligned}\int_0^C I_1(r_m,C)dC=\int_{r_m}^{\infty}dr\left(\left(\frac{\sqrt{C^2\sin^2\theta f(r)-\ell^2}}{\sin\theta\sqrt{f(r)}}-C\right)\right.\\\left.-\frac{i\ell}{\sin\theta\sqrt{f(r)}}\right)-C(r_m-r_h).\end{aligned} \tag{3.17}$$

Taking into account (3.14)–(3.17) we get the following relation between the quantities $S_{\rm NG}$ and L_ϕ

$$S_{\rm NG}^{\rm reg}=\frac{T}{\pi\alpha'}\frac{\ell}{C}\left(\frac{L_\phi}{2}+I_3(r_m,C)\right), \tag{3.18}$$

where

$$\begin{aligned}I_3(r_m,C)=\int_{r_m}^{\infty}dr\left(\frac{\sqrt{C^2\sin^2\theta f(r)-\ell^2}}{\ell\sin\theta\sqrt{f(r)}}-\frac{C}{\ell}\right)\\-\frac{C}{\ell}(r_m-r_h),\end{aligned} \tag{3.19}$$

and C is defined by (3.7).

Plugging (3.7), (3.18)–(3.19) into (2.17) and doing some algebra, we find the following relation for the quark-antiquark potential

$$\begin{aligned}V_{q\bar q}&=\frac{\sqrt{\lambda}}{\pi\ell^2}\sin\theta\sqrt{f(r_m)}\left(\frac{L_\phi}{2}+I_3\right),\\I_3&=\frac{1}{\sin\theta\sqrt{f(r_m)}}\left[\int_{r_m}^{\infty}\left(\sqrt{1-\frac{f(r_m)}{f(r)}}-1\right)dr\right.\\&\quad\left.-(r_m-r_h)\right],\end{aligned} \tag{3.20}$$

where $\sqrt{\lambda}=\ell^2/\alpha'$ and the distance between quarks L_ϕ is given by (3.10) with C defined in (3.7).

In Figs. 3 and 4 we present the numerical studies of the dependence of the quark-antiquark potential $V_{q\bar q}$ (3.12) on the distance L_ϕ (3.10). For all plots we perform numerical calculations at various temperatures keeping the 't Hooft coupling fixed as $\lambda=6\pi$ and varying the angle θ. In order to set the minimal Hawking temperature $T_{\rm H}^{\rm min}=0.16$ GeV, we put $\ell\approx 0.55$ fm. It worth to be mentioned, that the phase transition occurs at a slightly higher temperature, namely, at $T_{\rm c}=3/(2\pi\ell)\approx 0.17$ GeV.

The interquark distance L_ϕ (3.10) as a function of the integration constant C (3.7) is depicted in Fig. 3A. We observe that L_ϕ decreases as the temperature increases. One can also see that for a fixed temperature $T_{\rm H}$ the distance L_ϕ takes the smaller values while θ increases.

In Fig. 3B we show the distance between the quark-antiquark pair L_ϕ (3.10) as a function of the quantity $1-(r_h/r_m)^4$. This plot illustrates the dependence of the interquark separation L_ϕ on the turning point r_m. As in the previous plot we observe that the distance decreases with increasing temperature $T_{\rm H}$ and that the angle reduction leads to a decrease in the distance between quarks. In Fig. 3B we also see that L_ϕ increases until it reaches its maximal value $L_{\phi,\rm max}$ and then it decreases. It is interesting that one is able to obtain the same value of L_ϕ by tuning the temperature $T_{\rm H}$ and the angle θ.

The behavior of the quark-antiquark potential $V_{q\bar q}$ on the interquark distance L_ϕ is presented in Fig. 4A. For the plot we choose $T_{\rm H}=0.17$ GeV, that corresponds to the deconfined phase. We see that the quark-antiquark potential is double valued, however, the upper branch of the potential is

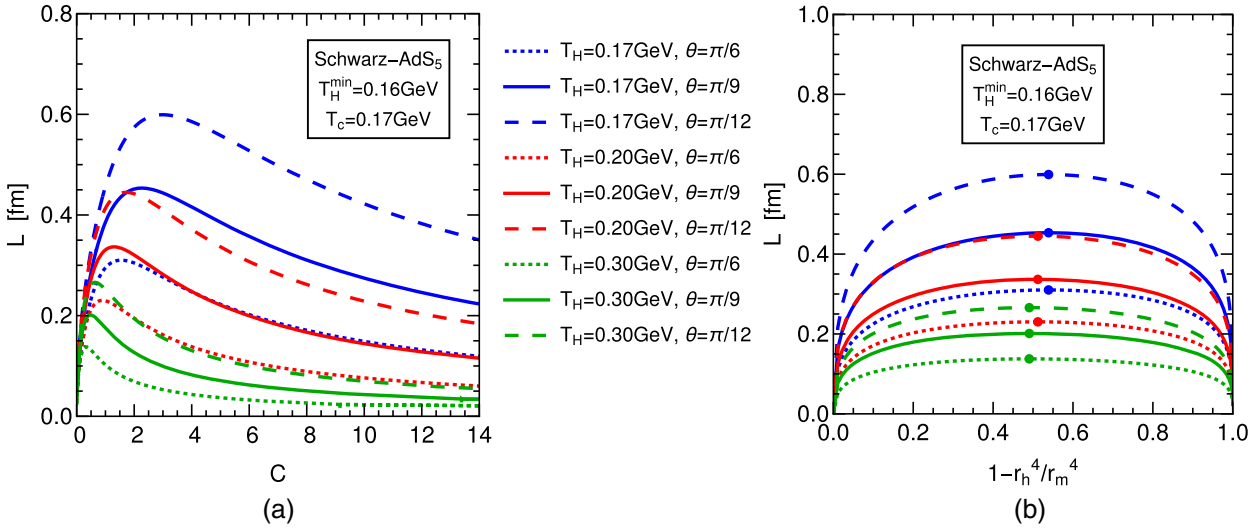

FIG. 3. (a) The distance between quark-antiquark pair L_ϕ as a function of the integration constant C (3.7). (b) The distance between quark-antiquark pair L_ϕ as a function of $1 - \frac{r_h^4}{r_m^4}$.

unphysical. It corresponds to an unfavorable string configuration in contrast to the lower branch, which is associated with the lower-energy string configuration. Note that at the distance $L_\phi = L_\phi(r_m)$ the potential $V_{q\bar{q}}$ tends to be zero and the configuration of two noninteracting straight strings is more preferable energetically. The same holds for $L_\phi > L_\phi(r_m)$. Thus, $L_\phi(r_m)$ can be interpreted as the screening length [23]. In the work [61] it was argued that the timelike screening length, which corresponds to the mean-free path for traveling "light" (gluon) in a medium, has the value $1/\pi T$. As we can see from Fig. 4A, this condition is satisfied for $\theta \gtrsim \pi/9$.

From Fig. 4A we see that the interquark potential has the Coulomb-like behavior. If we estimate (3.20), we find that $V_{q\bar{q}}$ has the Coulomb-like term. Indeed, the numerical evaluation of the term I_3 confirms that at small distances the contribution from I_3 is inversely proportional to the length $I_3 \sim -1/L_\phi$. We show the dependence I_3 as a function of $1/L_\phi$ in Fig. 4B. Note that I_3 is double valued because of the string configuration, see Fig. 3A. In the deconfined phase the string term vanishes. In our work we are able to approximate Eq. (3.20) as

$$V_{q\bar{q}}(L) = -\frac{\kappa}{L_\phi} + V_0. \tag{3.21}$$

However, in [62,63] it was suggested that in addition to the Coulomb contribution one has to include the medium-dependent term. In Table I we present values of κ and V_0, which obtained from fitting of $V_{q\bar{q}}$ in Fig. 4A. As one can

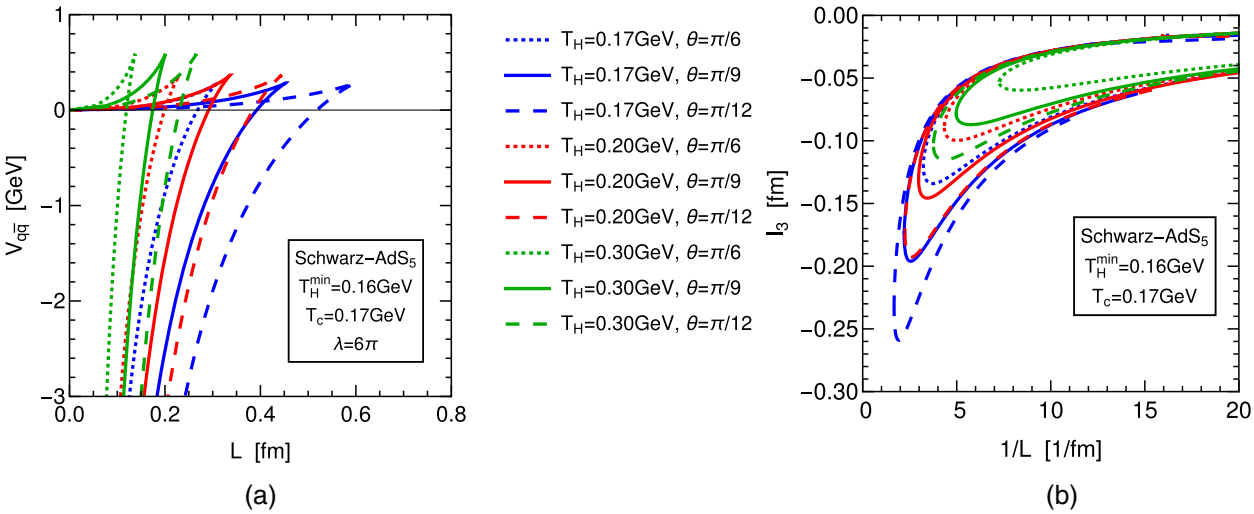

FIG. 4. (a) The quark-antiquark potential $V_{q\bar{q}}$ as a function of the distance L_ϕ. (b) The dependence of I_3 on the inverse distance $1/L_\phi$.

TABLE I. Fitting coefficients of $V_{q\bar{q}}$ (3.21) at temperatures $T_H = 0.17,\ 0.20,\ 0.30$ GeV and angles $\theta = \pi/6, \pi/9, \pi/12$, corresponding to Fig. 4.

T_H, GeV	θ	κ, GeV · fm	V_0, GeV
0.17	$\pi/6$	0.711459	2.67669
	$\pi/9$	1.04008	2.67669
	$\pi/12$	1.37443	2.67669
0.20	$\pi/6$	0.707247	3.6193
	$\pi/9$	1.03393	3.6193
	$\pi/12$	1.3663	3.6193
0.30	$\pi/6$	0.704129	6.08073
	$\pi/9$	1.02937	6.08073
	$\pi/12$	1.36027	6.08073

see, the constant V_0 does not depend on the angle θ, but it grows as the temperature T_H increases. Surprisingly, at the temperature just above the critical one, i.e., $T_H \approx 0.171$ GeV, the value of V_0 is equal to Euler's number. The Coulomb strength parameter κ weakly depends on T_H and increases with decreasing angle θ.

In Fig. 5 we compare our results for the potential in the Schwarzschild-AdS$_5$ background with $V_{q\bar{q}}$ in the planar AdS black hole [23]. For this we set $R = \ell$ in the planar AdS black hole case and fix $\theta = \pi/6$ for the Schwarzschild-AdS$_5$ background. We see that for the same quark-antiquark distance $V_{q\bar{q}}$ in Schwarzschild-AdS$_5$ (solid curves) takes greater values than the potential in the planar AdS background (dotted curves) [23]. This difference becomes more significant as the temperature increases.

B. Wilson loop in Kerr-AdS$_5$ black hole

Now we turn to the discussion of the holographic Wilson loop in the 5D Kerr-AdS black hole (2.7)–(2.8).

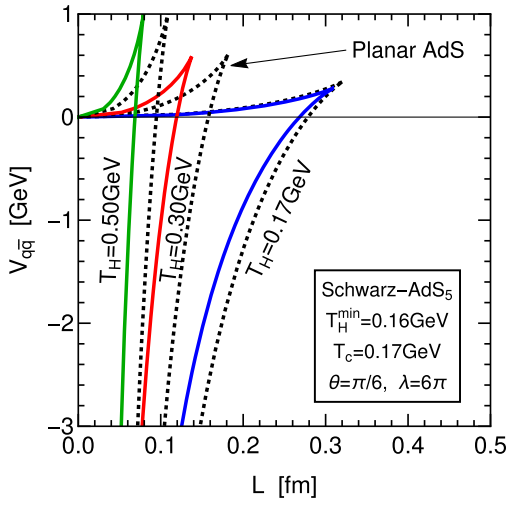

FIG. 5. $V_{q\bar{q}}$ in the Schwarzschild-AdS$_5$ (solid curves) and in the planar AdS (dotted curves) black holes at fixed $\theta = \pi/6$ and $T_H = 0.17,\ 0.30,\ 0.50$ GeV.

For the parametrization of the string world sheet we employ the following gauge condition:

$$\tau = T, \qquad \sigma = \Phi, \qquad y = y(\Phi), \qquad \Phi \in [0, 2\pi L_\Phi]. \tag{3.22}$$

The components of the induced metric (2.15) are

$$\begin{aligned} g_{\tau\tau} &= G_{TT} = -\left(1 + y^2\ell^{-2} - \frac{2M}{\Delta^3 y^2}\right), \\ g_{\tau\sigma} &= G_{T\Phi} = -\frac{2Ma\sin^2\Theta}{\Delta^3 y^2}, \\ g_{\sigma\sigma} &= G_{\Phi\Phi} + y'^2 G_{yy} = \sin^2\Theta\left(y^2 + \frac{2Ma^2\sin^2\Theta}{\Delta^3 y^2}\right) \\ &\quad + \frac{y'^2}{1 + y^2\ell^{-2} - \frac{2M}{\Delta^2 y^2}}, \end{aligned} \tag{3.23}$$

where Δ is given by (2.8) and we denoted $y' \equiv dy/d\Phi$. We also suppose the following boundary conditions for the location of the string endpoints

$$y\left(-\frac{L_\Phi}{2}\right) = y\left(\frac{L_\Phi}{2}\right) = \infty. \tag{3.24}$$

Taking into account (3.22)–(3.24) we write down the Nambu-Goto action in the following form:

$$S_{NG} = \frac{T}{2\pi\alpha'}\int_{-\frac{L_\Phi}{2}}^{\frac{L_\Phi}{2}} d\Phi \sqrt{y'^2\frac{f_{\Delta^3}(y)}{f_{\Delta^2}(y)} + y^2 F_{\Delta^3}(y)\sin^2\Theta}, \tag{3.25}$$

where for clarity we introduced the notation using dimensionless functions

$$\begin{aligned} f_{\Delta^2}(y) &= 1 + y^2\ell^{-2} - \frac{2M}{\Delta^2 y^2}, \\ f_{\Delta^3}(y) &= 1 + y^2\ell^{-2} - \frac{2M}{\Delta^3 y^2}, \\ F_{\Delta^3}(y) &= f_{\Delta^3}(y) + \frac{2Ma^2\sin^2\Theta}{y^4\Delta^3}(1 + y^2\ell^{-2}). \end{aligned} \tag{3.26}$$

The system (3.25) has the integral of motion

$$\mathcal{H} = -\frac{y^2 F_{\Delta^3}(y)\sin^2\Theta}{\sqrt{y'^2\frac{f_{\Delta^3}(y)}{f_{\Delta^2}(y)} + y^2 F_{\Delta^3}(y)\sin^2\Theta}}. \tag{3.27}$$

The turning point is defined by $y' = 0$, so from (3.27) we have

$$-y\sin\Theta\sqrt{F_{\Delta^3}(y)}|_{y=y_m}=-\frac{\ell}{C},\quad \text{with}\quad y_m=y(\Phi_m). \tag{3.28}$$

The equation of motion which follows from (3.27) is given by

$$y'^2=y^2F_{\Delta^3}(y)\frac{f_{\Delta^2}(y)}{f_{\Delta^3}(y)}\sin^2\Theta\left[\frac{C^2}{\ell^2}\sin^2\Theta y^2F_{\Delta^3}(y)-1\right]. \tag{3.29}$$

Substituting (3.29) into (3.25) and coming to the integration with respect to y one yields to the expression,

$$S_{\rm NG}=\frac{T}{\pi\alpha'}\int_{y_m}^{\infty}dy\frac{C\sin\Theta y\sqrt{F_{\Delta^3}(y)}}{\sqrt{C^2\sin^2\Theta y^2F_{\Delta^3}(y)-\ell^2}}\sqrt{\frac{f_{\Delta^3}(y)}{f_{\Delta^2}(y)}}. \tag{3.30}$$

Equation (3.30) is divergent at the conformal boundary $y\to+\infty$ of the Kerr-AdS$_5$ black hole.

Just like in the Schwarzschild-AdS case, the renormalization procedure is a subtraction of the single quarks "self-energy", which is represented by the action of a static straight string in Kerr-AdS$_5$,

$$S_0=\frac{T}{\pi\alpha'}\int_{y_+}^{\infty}dy\sqrt{-G_{TT}G_{yy}}=\frac{T}{\pi\alpha'}\left(\int_{y_m}^{\infty}+\int_{y_+}^{y_m}\right)\times\sqrt{\frac{f_{\Delta^3}(y)}{f_{\Delta^2}(y)}}dy. \tag{3.31}$$

Subtracting (3.31) from (3.30) we get

$$S_{\rm NG}^{\rm ren}=\frac{T}{\pi\alpha'}\left[\int_{y_m}^{\infty}dy\sqrt{\frac{f_{\Delta^3}(y)}{f_{\Delta^2}(y)}}\left(\frac{C\sin\Theta y\sqrt{F_{\Delta^3}(y)}}{\sqrt{C^2\sin^2\Theta y^2F_{\Delta^3}(y)-\ell^2}}-1\right)-\int_{y_+}^{y_m}dy\sqrt{\frac{f_{\Delta^3}(y)}{f_{\Delta^2}(y)}}\right]. \tag{3.32}$$

From Eq. (3.29) we find the interquark distance L_Φ,

$$\frac{L_\Phi}{2}=\int_{y_m}^{\infty}dy\frac{\ell}{\sin\Theta y\sqrt{F_{\Delta^3}(y)}\sqrt{C^2\sin^2\Theta y^2F_{\Delta^3}(y)-\ell^2}}\times\sqrt{\frac{f_{\Delta^3}(y)}{f_{\Delta^2}(y)}}. \tag{3.33}$$

As in the previous subsection one can find the relation between the string action (3.30) and the quark-antiquark distance (3.33). For this reason, we define (3.32) and (3.33)

$$S_{\rm NG}^{\rm ren}=\frac{T}{\pi\alpha'}I_1(y_m,C),\qquad \frac{L_\Phi}{2}=I_2(y_m,C). \tag{3.34}$$

Correspondingly, derivatives of $I_1(y_m,C)$ and $I_2(y_m,C)$ (3.34) with respect to C are

$$\frac{\partial I_1(y_m,C)}{\partial C}=-\int_{y_m}^{\infty}dy\frac{y\ell^2\sin\Theta\sqrt{F_{\Delta^3}(y)}}{(\sin^2\Theta C^2y^2F_{\Delta^3}(y)-\ell^2)^{3/2}}\times\sqrt{\frac{f_{\Delta^3}(y)}{f_{\Delta^2}(y)}}, \tag{3.35}$$

$$\frac{\partial I_2(y_m,C)}{\partial C}=-\int_{y_m}^{\infty}dy\frac{yC\ell\sin\Theta\sqrt{F_{\Delta^3}(y)}}{(\sin^2\Theta C^2y^2F_{\Delta^3}(y)-\ell^2)^{3/2}}\times\sqrt{\frac{f_{\Delta^3}(y)}{f_{\Delta^2}(y)}}. \tag{3.36}$$

Comparing (3.35) with (3.36), we find the following relation:

$$\frac{\partial I_2(y_m,C)}{\partial C}=\frac{C}{\ell}\frac{\partial I_1(y_m,C)}{\partial C}. \tag{3.37}$$

Integrating the lhs of Eq. (3.37), we obtain

$$\int_0^C\frac{\partial I_2(y_m,C)}{\partial C}dC=\frac{L_\Phi}{2}+I_{\Delta^3}, \tag{3.38}$$

where we use the notation

$$I_{\Delta^3}=i\int_{y_m}^{\infty}\frac{dy}{\sin\Theta y\sqrt{F_{\Delta^3}(y)}}\sqrt{\frac{f_{\Delta^3}(y)}{f_{\Delta^2}(y)}}. \tag{3.39}$$

At the same time, integrating the rhs of Eq. (3.37) by parts, we come to

$$\int_0^C C\frac{\partial I_1(y_m,C)}{\partial C}dC=CI_1(y_m,C)-\int_0^C I_1(y_m,C)dC. \tag{3.40}$$

The latter integral can be easily found

$$\int_0^C I_1(y_m,C)dC=\int_{y_m}^{\infty}dy\frac{\sqrt{C^2\sin^2\Theta y^2F_{\Delta^3}(y)-\ell^2}}{\sin\Theta y\sqrt{F_{\Delta^3}(y)}}\times\sqrt{\frac{f_{\Delta^3}(y)}{f_{\Delta^2}(y)}}-C\int_{y_+}^{y_m}dy\sqrt{\frac{f_{\Delta^3}(y)}{f_{\Delta^2}(y)}}-I_{\Delta^3}\ell. \tag{3.41}$$

Now collecting Eqs. (3.37)–(3.41), we get

$$S_{\rm NG}^{\rm ren}=\frac{\ell}{C}\frac{T}{\pi\alpha'}\left(\frac{L_\Phi}{2}+I_3\right), \tag{3.42}$$

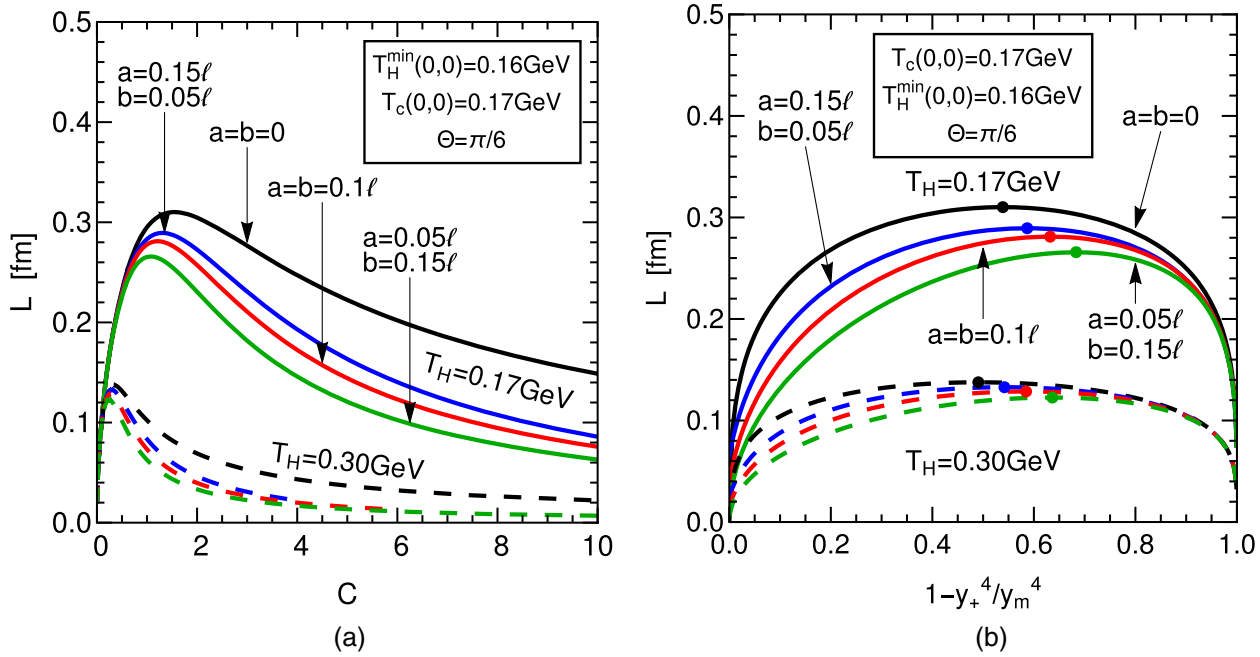

FIG. 6. (a) The behavior of the interquark distance L_Φ on the integration constant C (3.28). (b) L_Φ as a function of $1-\frac{y_+^4}{y_m^4}$.

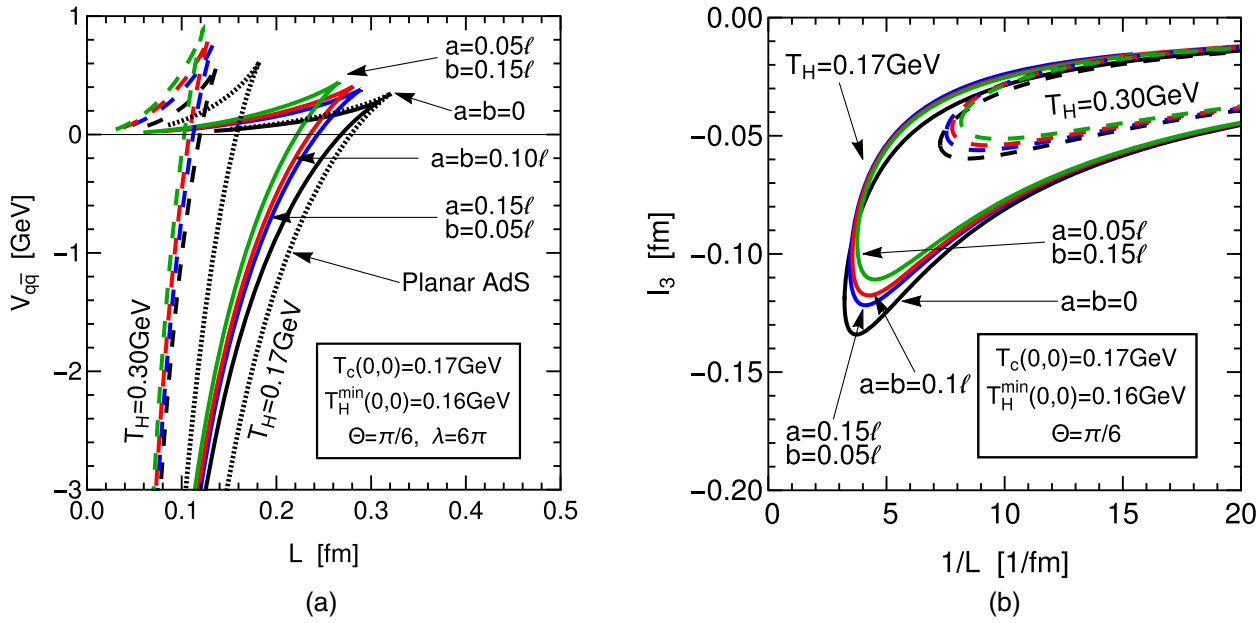

FIG. 7. (a) The dependence of the quark-antiquark potential $V_{q\bar{q}}$ on the distance L_Φ. (b) The behavior of $\mathcal{I}_3$ (3.43) on the inverse length $1/L_\Phi$.

where

$$I_3=\int_{y_m}^{\infty}dy\sqrt{\frac{f_{\Delta^3}(y)}{f_{\Delta^2}(y)}}\left(\frac{\sqrt{C^2\sin^2\Theta y^2F_{\Delta^3}(y)-\ell^2}}{y\sin\Theta\sqrt{F_{\Delta^3}(y)}}-C\right)-\frac{C}{\ell}\times\int_{y_+}^{y_m}dy\sqrt{\frac{f_{\Delta^3}(y)}{f_{\Delta^2}(y)}}. \tag{3.43}$$

So, taking into account (3.43), we find the same expression as (3.20) for the quark-antiquark potential

$$V_{q\bar{q}}=\frac{\sqrt{\lambda}}{\pi\ell^2}y_m\sin\Theta\sqrt{F_{\Delta^3}(y_m)}\left(\frac{L_\Phi}{2}+I_3\right). \tag{3.44}$$

Figs. 6A–6B show the dependences of the interquark distance L_Φ (3.33) on the constant C (3.28) and the quantity

TABLE II. Fitting coefficients in the (3.20) at temperatures $T_{\rm H}=0.17$ GeV and $T_{\rm H}=0.30$ GeV, $\Theta=\pi/6$ and rotational parameters are fixed as in Fig. 7A.

$T_{\rm H}$, GeV	a/ℓ	b/ℓ	κ, GeV · fm	V_0, GeV
0.17	0	0	0.711459	2.67669
	0.15	0.05	0.711887	2.95381
	0.1	0.1	0.711556	3.05421
	0.05	0.15	0.710322	3.23494
0.30	0	0	0.704129	6.08073
	0.15	0.05	0.702162	6.39186
	0.1	0.1	0.701980	6.62686
	0.05	0.15	0.701468	6.96067

$1-\frac{y_+^4}{y_m^4}$, respectively. In the plots, the temperature $T_{\rm H}$ and the value of the angle Θ are fixed, while we vary the rotational parameters a and b. In both Figs. 6A and 6B we see that L_Φ decreases as the rotational parameters increase, so the interquark distance has the bigger values for zero rotational parameters.

The dependence of the potential $V_{q\bar{q}}$ on the interquark distance L_Φ is shown in Fig. 7A. We set $T_{\rm H}=0.17$ GeV and $\lambda=6\pi$. From Fig. 7A we see that $V_{q\bar{q}}$ is double valued, but only the lower curve is significant as for the nonrotating case. This branch corresponds to the string configuration with the lower energy. The potential $V_{q\bar{q}}$ crosses zero at $L_{\Phi,m}=L_\Phi(y_m)$, which can be interpreted as the screening length. The upper branch of the potential, which starts at $L_{\Phi,m}$, is related to a configuration of two separated straight strings. We can observe in Fig. 7A that at $T_{\rm H}=0.17$ GeV the potential $V_{q\bar{q}}$ for nonzero rotational parameters (color solid curves) can have greater values than in Schwarzschild-AdS$_5$ (black solid curve). Increasing the temperature $T_{\rm H}=0.3$ GeV the potential $V_{q\bar{q}}$ in Kerr-AdS$_5$ comes closer to $V_{q\bar{q}}$ in the Schwarzschild-AdS$_5$ black hole. It should be noted that the same values of $V_{q\bar{q}}$ at different temperatures corresponds to different L_Φ, which decreases as the temperature increases.

From Fig. 7A one can see that the potential has also the Coulomb form, which is similar to the Schwarzschild-AdS case. This is also confirmed by the dependence of the I_3-term on the inverse interquark distance $1/L$ depicted in Fig. 7B. Note that in [24] it was shown that the quark-antiquark potential in the rotating D3-brane interpolates between the Coulomb and confining parts.

We are able to find an approximation of $V_{q\bar{q}}$ (3.44) assuming that above the critical temperature $T_{\rm H}=0.17$ GeV it is given by (3.21). We write down κ and V_0 for various values of the rotational parameters a and b in Table II.

We see that the Coulomb strength parameter κ weakly depends on the rotational parameters (at least for values of a and b under consideration) and on the temperature. On the contrary, the term V_0 strongly depends on the rotation and $T_{\rm H}$.

IV. JET-QUENCHING PARAMETER

A. Jet-quenching parameter in the 5D Schwarzschild-AdS black hole

In this section, we will discuss the jet-quenching parameter in the 5D Schwarzschild-AdS background (2.3)–(2.4) following the holographic prescription.

To find the jet-quenching parameter $\hat{q}$ we have to come to the scaled "light cone" coordinates

$$dx^+=\ell^2(dt-\ell d\phi),\qquad dx^-=\ell^2(dt+\ell d\phi). \tag{4.1}$$

By virtue of the transformations (4.1) we come to the following form of the Schwarzschild-AdS$_5$ metric (2.3)

$$\begin{aligned}ds^2=&\frac{1}{4\ell^4}\left(\frac{r^2}{\ell^2}\sin^2\theta-\frac{f(r)}{r^2}\right)[(dx^-)^2+(dx^+)^2]\\&-\frac{1}{2\ell^4}\left(\frac{r^2}{\ell^2}\sin^2\theta+\frac{f(r)}{r^2}\right)dx^-dx^+\\&+\frac{r^2}{f(r)}dr^2+r^2d\theta^2+r^2\cos^2\theta d\psi^2,\end{aligned} \tag{4.2}$$

where $f(r)$ is given by (2.4). We have to study a holographic lightlike Wilson loop (2.20) in the background (4.2). We choose the coordinates on the string world sheet as follows:

$$\tau=x^-,\qquad \sigma=\psi. \tag{4.3}$$

Moreover, for the string configuration we also suppose

$$x^\mu=x^\mu(\sigma),\qquad \theta(\sigma)=\text{const},\qquad x^+(\sigma)=\text{const}. \tag{4.4}$$

Taking into account (4.3)–(4.4) we find the corresponding Nambu-Goto action (2.14)

$$\begin{aligned}S=&\frac{L^-}{2\pi\alpha'}\int_{-L/2}^{L/2}d\psi\,\frac{r}{2\ell^2}\\&\times\sqrt{\left(\frac{f(r)}{r^2}-\ell^{-2}r^2\sin^2\theta\right)\left(\cos^2\theta+\frac{r'^2}{f(r)}\right)},\end{aligned} \tag{4.5}$$

where we define $r' \equiv \partial r/\partial\psi$. The corresponding first integral is given by

$$\mathcal{H} = -\frac{\cos^2\theta\sqrt{f(r) - r^4\ell^{-2}\sin^2\theta}}{2\ell^2\sqrt{\cos^2\theta + \frac{r'^2}{f(r)}}}. \tag{4.6}$$

From (4.6) we find the equation of motion

$$r'^2 = \frac{f(r)\cos^2\theta}{4C^2\ell^6}[\cos^2\theta(f(r)\ell^2 - r^4\sin^2\theta) - 4C^2\ell^6], \tag{4.7}$$

where C is some constant. Plugging (4.7) into (4.5) and integrating with respect to r the Nambu-Goto action can be represented as

$$S = \frac{L^-}{\pi\alpha'}\int_{r_h+\epsilon}^{\infty} dr \times \frac{\cos\theta(f(r)\ell^2 - r^4\sin^2\theta)}{2\ell^3\sqrt{f(r)}\sqrt{\cos^2\theta(f(r)\ell^2 - r^4\sin^2\theta) - 4C^2\ell^6}}. \tag{4.8}$$

The relation (4.8) is divergent on the background boundary $r \to +\infty$ and has to be renormalized. Moreover, since Eq. (4.8) contains a multiplier $f(r)^{-1/2}$ we regularize the action on the lower bound as $r_h + \epsilon$. The normalization of Eq. (4.8) can be performed through the subtraction of the static mass of the quark and antiquark, which is given by

$$S_0 = \frac{L^-}{\pi\alpha'}\int_{r_h+\epsilon}^{\infty} dr\frac{\sqrt{f(r)\ell^2 - r^4\sin^2\theta}}{2\ell^3\sqrt{f(r)}}. \tag{4.9}$$

With (4.9) the regularized string action is given by

$$S^{\text{reg}} = S - S_0 = \frac{L^-}{\pi\alpha'}\int_{r_h+\epsilon}^{\infty} dr\frac{\sqrt{f(r)\ell^2 - r^4\sin^2\theta}}{2\ell^3\sqrt{f(r)}} \times \left(\frac{\cos\theta\sqrt{f(r)\ell^2 - r^4\sin^2\theta}}{\sqrt{\cos^2\theta(f(r)\ell^2 - r^4\sin^2\theta) - 4C^2\ell^6}} - 1\right). \tag{4.10}$$

Expanding (4.10) for small C (in the low-energy limit) we find

$$S^{\text{reg}} = \frac{L^-}{\pi\alpha'}\frac{\ell^2C^2}{\cos^2\theta}\mathcal{I}, \tag{4.11}$$

where we denote by $\mathcal{I}$ by the following integral:

$$\mathcal{I} = \int_{r_m}^{\infty}\frac{dr}{\sqrt{f(r)}\sqrt{f(r) - r^4\ell^{-2}\sin^2\theta}} \tag{4.12}$$

and r_m is defined as a positive real solution to the equation

$$r^2 + r^4\ell^{-2}\cos^2\theta - 2M = 0. \tag{4.13}$$

To find the relation between L and C we remember that $r(\pm L/2) = \infty$ and we have

$$\frac{L}{2} = \frac{2C\ell^3}{\cos\theta}\int_{r_h}^{\infty}\frac{dr}{\sqrt{f(r)}\sqrt{\cos^2\theta(f(r)\ell^2 - r^4\sin^2\theta) - 4C^2\ell^6}}, \tag{4.14}$$

or for small C we get

$$\frac{L}{2} = \frac{2\ell^2C}{\cos^2\theta}\mathcal{I}. \tag{4.15}$$

Deriving C from (4.15) and substituting into the action (4.11) we come to

$$S^{\text{reg}} = \frac{L^-}{\pi\alpha'}\frac{L^2\cos^2\theta}{16\ell^2\int_{r_m}^{\infty}\frac{dr}{\sqrt{f(r)}\sqrt{f(r) - r^4\ell^{-2}\sin^2\theta}}}. \tag{4.16}$$

We note that $r_m \geq r_h$ and r_m coincides with r_h only for $\theta = 0$. In this case we need to shift the turning point to regularize the divergence near r_h, i.e., $r_m|_{\theta=0} = r_h + \epsilon$.

Taking into account (2.23) and (4.16), we find the jet-quenching parameter

$$\hat{q} = \frac{\sqrt{\lambda}}{\sqrt{2}\pi}\frac{\cos^2\theta}{\ell^4\int_{r_m}^{\infty}\frac{dr}{\sqrt{f(r)}\sqrt{f(r) - r^4\ell^{-2}\sin^2\theta}}}, \tag{4.17}$$

with $\lambda = \ell^4/\alpha'^2$ and $f(r)$ given by (2.4).

We are not able to calculate (4.17) analytically. However, for small θ and $\ell = 1$ we can estimate the expression for $\hat{q}$. First, we find the integral in the denominator of (4.17) for $\ell = 1$ and small θ

$$\int_{r_h+\epsilon}^{\infty}\frac{dr}{r^4+r^2-2M}=\left(\frac{\ln\left(\frac{2r-\sqrt{2}\sqrt{\sqrt{8M+1}-1}}{2r+\sqrt{2}\sqrt{\sqrt{8M+1}-1}}\right)}{\sqrt{2}\sqrt{8M+1}\sqrt{\sqrt{8M+1}-1}}-\frac{\sqrt{2}\arctan\left(\frac{\sqrt{2}r}{\sqrt{\sqrt{8M+1}+1}}\right)}{\sqrt{8M+1}\sqrt{\sqrt{8M+1}+1}}\right)\Bigg|_{r_h+\epsilon}^{\infty}$$
$$=\frac{1}{(1+2r_h^2)\sqrt{1+r_h^2}}\left(\arctan\left(\frac{r_h}{\sqrt{r_h^2+1}}\right)-\frac{\pi}{2}-\frac{\ln\left(\frac{\epsilon}{\epsilon+2r_h}\right)\sqrt{r_h^2+1}}{2r_h}+\frac{\ln(\infty)\sqrt{r_h^2+1}}{2r_h}\right)$$
$$=\frac{\sqrt{2}}{(\pi^2T_{\rm H}^2+\pi T_{\rm H}\sqrt{\pi^2T_{\rm H}^2-2})\sqrt{\pi T_{\rm H}(\sqrt{\pi^2T_{\rm H}^2-2}+\pi T_{\rm H})+1}}$$
$$\times\left(-\operatorname{arccot}\left(\frac{\pi T_{\rm H}+\sqrt{\pi^2T_{\rm H}^2-2}}{\sqrt{2}\sqrt{\pi T_{\rm H}(\sqrt{\pi^2T_{\rm H}^2-2}+\pi T_{\rm H})+1}}\right)\right.$$
$$\left.+\frac{\sqrt{\pi T_{\rm H}(\sqrt{\pi^2T_{\rm H}^2-2}+\pi T_{\rm H})+1}\left(\ln(\infty)-\ln\left(\frac{\epsilon}{\epsilon+2r_h}\right)\right)}{\sqrt{2}(\pi T_{\rm H}+\sqrt{\pi^2T_{\rm H}^2-2})}\right). \tag{4.18}$$

Thus, for high temperatures, $\ell=1$, and small θ we get the dependence $\hat{q}$ on the temperature as for the planar AdS black brane [54]

$$\hat{q}\sim\frac{\sqrt{\lambda}}{2\pi}\kappa T_{\rm H}^3, \tag{4.19}$$

where κ is some constant.

In Fig. 8A we show the jet-quenching parameter $\hat{q}$ (4.17) for different θ (solid curves) as a function of the temperature $T_{\rm H}$.

Note that we are able to trace the behavior of $\hat{q}$ starting from the $T_{\rm H}^{\rm min}$, since below this temperature the black hole does not exist. From Fig. 8A we see that for small values of the angle θ, the parameter $\hat{q}$ is quite close to the curve $\hat{q}_{\rm SYM}$ [see Eq. (1.1)] corresponding to the planar AdS_5 black brane from [54]. It is interesting that we can find a small value of θ, for instance $\theta<\pi/9$, such that the jet-quenching parameter $\hat{q}$ is even smaller than $\hat{q}_{\rm SYM}$ for all values of $T_{\rm H}$. Thus, we see that the value of the jet-quenching parameter for the Schwarzschild-AdS black hole depends on the location of the quark.

The fact that $\hat{q}$ in the Schwarzschild-AdS background for very small angles θ can lie below the curve $\hat{q}_{\rm SYM}$ in the AdS black brane background is explained by that we have the different contributions of the metric coefficients for the AdS_5 black holes with planar and spherical horizons. Taking $\theta\sim 0$ we change the contribution from the $G_{x^-x^-}$ term (4.2) in the Nambu-Goto action (4.5).

It is instructive to look on the dependence of $\hat{q}/T_{\rm H}^3$ on the ratio $T_{\rm H}/T_{\rm H}^{\rm min}$. We depict this for the Schwarzschild-AdS black hole (solid curves) and AdS black brane (dashed curve) in Fig. 8B. Comparing to $\hat{q}_{\rm SYM}/T_{\rm H}^3$, which is constant for all range of $T_{\rm H}/T_{\rm H}^{\rm min}$, the quantity $\hat{q}/T_{\rm H}^3$ for the Schwarzschild-AdS_5 background has a nonlinear behavior on $T_{\rm H}$ up to some value of $T_{\rm H}$, above which it also takes a constant value. From this figure, one can conclude that at high temperature the jet-quenching parameter $\hat{q}$ in the AdS black hole has a generic dependence on $T_{\rm H}$ as $T_{\rm H}^3$.

B. Jet-quenching parameter in the Kerr-AdS$_5$ background

Now we turn to the calculation of the jet-quenching parameter $\hat{q}$ in the Kerr-AdS_5 background (2.7) with two arbitrary rotational parameters. Here we use the following "light cone" coordinates suggested in [64]

$$dx^+=dT-ad\Phi,\qquad dx^-=dT+ad\Phi. \tag{4.20}$$

Taking into account (4.20) and putting for simplicity $\ell=1$ the Kerr-AdS_5 metric (2.7) takes the form,

$$ds^2\simeq\frac{1}{4}\zeta(y)(dx^-)^2+\frac{1}{4}\left(\eta(y)+\frac{2M}{\Delta^3y^2}(1+\sin^2\Theta)^2\right)(dx^+)^2$$
$$+\frac{1}{2}\left(\xi(y)+\frac{2M}{\Delta^3y^2}(1-\sin^4\Theta)\right)dx^-dx^+$$
$$-\frac{2M}{\Delta^3y^2}b(1-\sin^4\Theta)d\Psi dx^+-\frac{2M}{\Delta^3y^2}b\cos^4\Theta d\Psi dx^-$$
$$+\cos^2\Theta\left(y^2+\frac{2M}{\Delta^3y^2}b^2\cos^2\Theta\right)d\Psi^2+\frac{dy^2}{f_{\Delta^2}(y)}+y^2d\Theta^2, \tag{4.21}$$

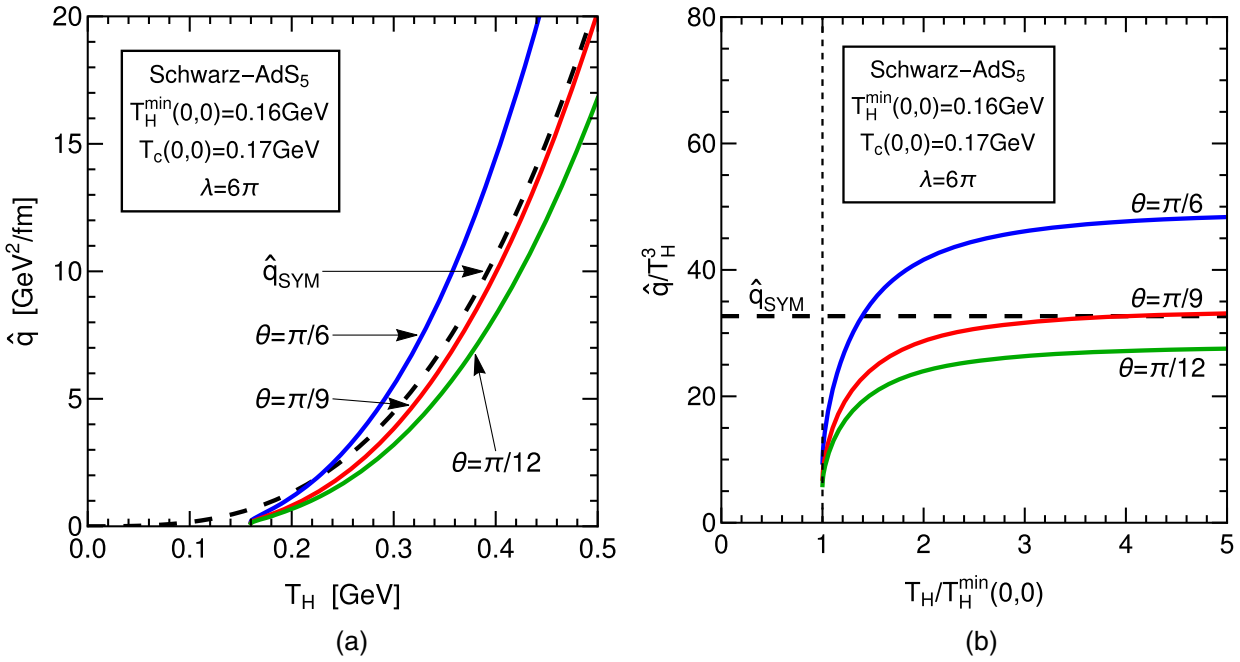

FIG. 8. (a) The dependence of $\hat{q}$ on the temperature T_{H} for different values of θ. The case $\hat{q}_{\mathrm{SYM}}$ for the planar AdS_5 black brane [see Eq. (1.1)] is shown by the black dashed curve. (b) $\hat{q}/T_{\mathrm{H}}^3$ as a function of $T_{\mathrm{H}}/T_{\mathrm{H}}^{\mathrm{min}}$ for different values of θ. The case $\hat{q}_{\mathrm{SYM}}$ for the planar AdS_5 black brane is shown by the black dashed line.

where $f_{\Delta^2}(y)$ is given by (3.26), and we introduced the following notation:

$$\eta(y) = 1 + y^2 - \frac{y^2}{a^2}\sin^2\Theta,$$
$$\xi(y) = -(1 + y^2) - \frac{y^2}{a^2}\sin^2\Theta,$$
$$\zeta(y) = \eta(y) - \frac{2M}{\Delta^3 y^2}\cos^4\Theta. \tag{4.22}$$

We parametrize the string world sheet as follows:

$$\tau = x^-, \qquad \sigma = \Psi, \tag{4.23}$$

so L is a length along Ψ and we have L^- along the light cone direction. We also suppose that

$$x^\mu = x^\mu(\sigma), \tag{4.24}$$

thus the Wilson loop lies at constant x^+ and Θ

$$\Theta(\sigma) = \text{const}, \qquad x^+(\sigma) = \text{const}. \tag{4.25}$$

We also impose the following constraint for the string endpoints

$$y(\pm L/2) = \infty, \tag{4.26}$$

and

$$y(\sigma) = y(-\sigma). \tag{4.27}$$

The string dynamics in the background (4.21) is governed by the Nambu-Goto action (2.14) defined as

$$S = \frac{L^-}{2\pi\alpha'}\int_0^{\Psi} d\Psi \frac{1}{2\ell^2}\sqrt{\frac{y'^2\zeta(y)}{f_{\Delta^2}(y)} + \beta(y)}, \tag{4.28}$$

where for simplicity we introduce

$$\beta(y) = \cos^2\Theta\left(\eta(y)\frac{2M}{\Delta^3 y^2}b^2\cos^2\Theta + \zeta(y)y^2\right) \tag{4.29}$$

and $y' \equiv \frac{dy}{d\Psi}$. The integral of motion, which follows from (4.28), is given by

$$\mathcal{H} = \frac{\beta(y)}{2\sqrt{\beta(y) + \frac{y'^2\zeta(y)}{f_{\Delta^2}(y)}}}. \tag{4.30}$$

From (4.30) one obtains the equation of motion

$$y'^2 = \frac{f_{\Delta^2}(y)\beta(y)}{\zeta(y)}\left(\frac{\beta(y)}{4C^2} - 1\right). \tag{4.31}$$

By owning (4.31), we find the Nambu-Goto action (4.28) in terms of the holographic coordinate y

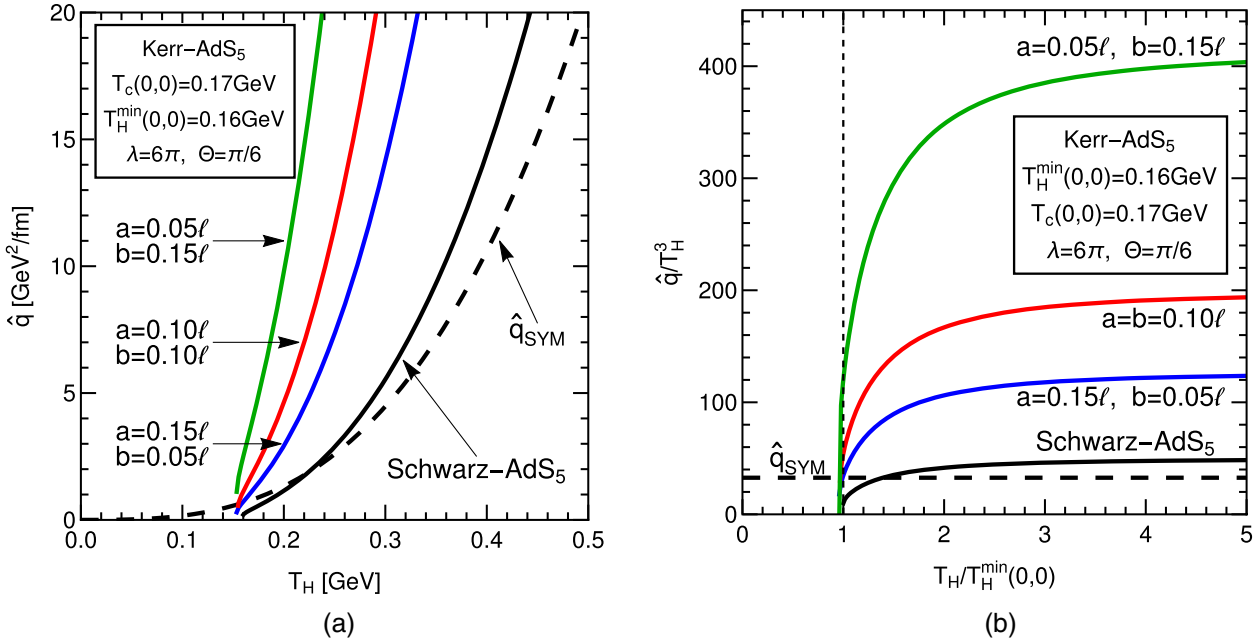

FIG. 9. (a) The jet-quenching parameter $\hat{q}$ as a function of $T_{\rm H}$ in the Kerr-AdS$_5$ geometry at different rotational parameters (color solid curves), in the AdS black hole with a planar horizon (the dashed curve) and in the Schwarzschild-AdS$_5$ background (the solid black curve). (b) $\hat{q}/T_{\rm H}^3$ as a function of $T_{\rm H}/T_{\rm H}^{\rm min}$ for different values of rotational parameters.

$$S=\frac{L^-}{\pi\alpha'}\int_{y_+}^{\infty}dy\frac{\sqrt{\zeta(y)\beta(y)}}{2\sqrt{f_{\Delta^2}(y)(\beta(y)-4C^2)}}. \tag{4.32}$$

As in the nonrotating case considered in the previous section the string action Eq. (4.32) has a divergence near the boundary $y\to+\infty$. To renormalize it one has to subtract the "self-energy" of two quarks, i.e., the action of two straight strings in the background (4.21),

$$S_0=\frac{L^-}{\pi\alpha'}\int_{y_+}^{\infty}dy\sqrt{|G_{x^-x^-}G_{yy}|}=\frac{L^-}{\pi\alpha'}\int_{y_+}^{\infty}\frac{\sqrt{\zeta(y)}}{2\sqrt{f_{\Delta^2}(y)}}. \tag{4.33}$$

The regularized Nambu-Goto action (4.32) is given by

$$S^{\rm reg}=S-S_0=\frac{L^-}{\pi\alpha'}\int_{y_+}^{\infty}dy\frac{\sqrt{\zeta(y)}}{2\sqrt{f_{\Delta^2}(y)}}\left(\frac{\sqrt{\beta(y)}}{\sqrt{\beta(y)-4C^2}}-1\right). \tag{4.34}$$

To find a relation between the constant C and the interquark distance L, we can use the relation (4.31),

$$\frac{L}{2}=\int_{y_+}^{\infty}dy\frac{2C\sqrt{\zeta(y)}}{\sqrt{f_{\Delta^2}(y)\beta(y)}\sqrt{\beta(y)-4C^2}}. \tag{4.35}$$

In the limit for small C the Nambu-Goto action (4.34) and the distance L between string endpoints (4.35) take the following form:

$$S^{\rm reg}=\frac{L^-}{\pi\alpha'}C^2\mathcal{I}+\mathcal{O}(C^4), \tag{4.36}$$

$$\frac{L}{2}=2C\mathcal{I}+\mathcal{O}(C^3), \tag{4.37}$$

where for convenience we introduce

$$\mathcal{I}=\int_{y_+}^{\infty}dy\frac{\sqrt{\zeta(y)}}{\beta(y)\sqrt{f_{\Delta^2}(y)}}, \tag{4.38}$$

with $f_{\Delta^2}(y)$, $\zeta(y)$, and $\beta(y)$ are given by (3.26), (4.22), and (4.29), respectively. Finally, plugging (4.37) into (4.36) we find that the Nambu-Goto action is

$$S^{\rm reg}=\frac{L^-}{\pi\alpha'}\frac{L^2}{16\mathcal{I}}. \tag{4.39}$$

Correspondingly, by owning (2.23) the jet-quenching parameter $\hat{q}$ in the Kerr-AdS$_5$ background can be read off as follows:

$$\hat{q}=\frac{\sqrt{\lambda}}{\sqrt{2}\pi\mathcal{I}}, \tag{4.40}$$

or restoring the dimension with ℓ one can write $\hat{q}=\frac{\sqrt{\lambda}}{\sqrt{2}\pi\ell^4\mathcal{I}}$.

In Fig. 9A we show the behavior of the jet-quenching parameter $\hat{q}$ in the Kerr-AdS$_5$ background (4.40) as a function of $T_{\rm H}$ for different rotational parameters a and b (color solid curves). From this figure we find that nonzero

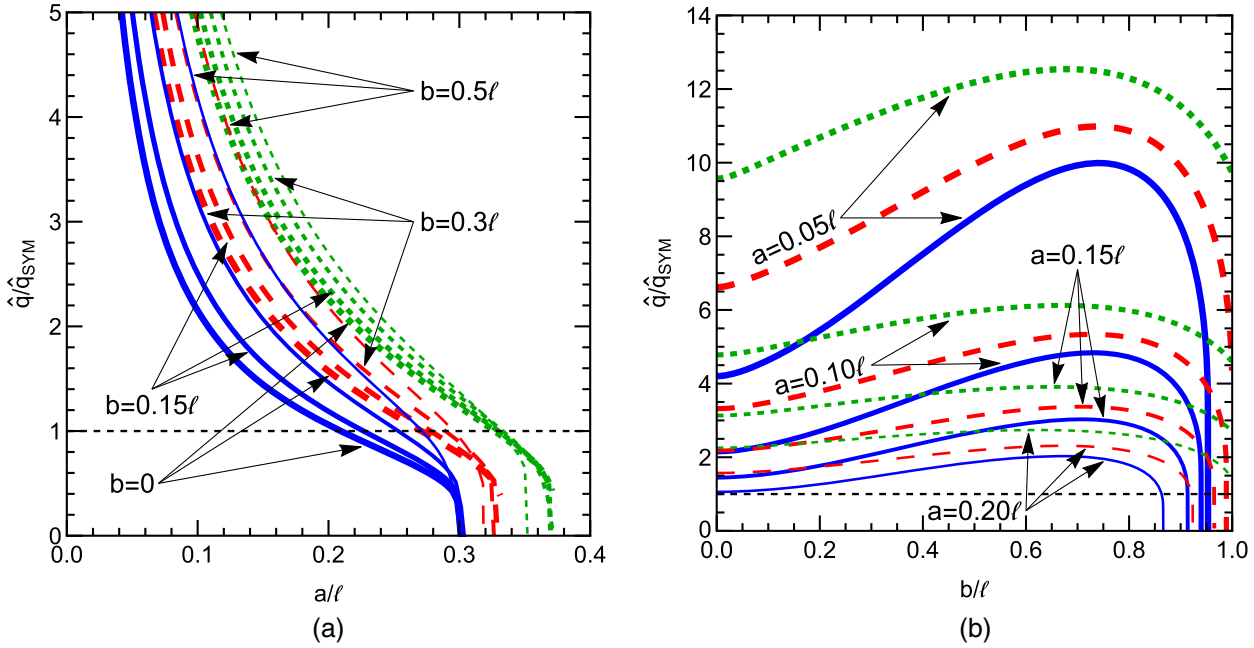

FIG. 10. (a) The dependence of the ratio $\hat{q}$ in the Kerr-AdS$_5$ to $\hat{q}_{\rm SYM}$ in the planar AdS black hole on the rotational parameter a for different b and $T_{\rm H}$; $T_{\rm H}=0.17$ GeV (solid blue), $T_{\rm H}=0.20$ GeV (dashed red), $T_{\rm H}=0.30$ GeV (dotted green). (b) $\hat{q}/\hat{q}_{\rm SYM}$ as a function of the rotational parameter b for different a and $T_{\rm H}$. The rotational parameter a is fixed as $a=0.20\ell$ for $T_{\rm H}=0.17$, 0.20, 0.30 GeV.

rotational parameters increase $\hat{q}$ comparing to $\hat{q}_{\rm SYM}$, which is calculated in the planar AdS black brane background. However, it is worth noting that for $a<b$ the value of the jet-quenching parameter $\hat{q}$ is greater than for $a\geq b$. We see that $\hat{q}$ increases with the temperature faster in the Kerr-AdS background then in the nonrotating AdS black hole, so one can say that the rotation promotes to the energy loss.

The dependence $\hat{q}/T_{\rm H}^3$ on $T_{\rm H}/T_{\rm H}^{\rm min}(0,0)$ for the Kerr-AdS$_5$ background is depicted in Fig. 9B. We observe that $\hat{q}/T_{\rm H}^3$ increases up to some value of $T_{\rm H}$, above which it becomes a constant similar to the case of the Schwarzschild-AdS black hole. Therefore, at high temperatures the jet-quenching parameter $\hat{q}$ is proportional to $T_{\rm H}^3$ as in the Schwarzschild-AdS$_5$ (4.19) and the planar cases (1.1) [54]

$$\hat{q}\sim\kappa_{\rm rot}T_{\rm H}^3, \tag{4.41}$$

where the coefficient $\kappa_{\rm rot}$ depends on values of a and b.

It is instructive to see the ratio $\hat{q}/\hat{q}_{\rm SYM}$ in terms of a rotational parameter. In Figs. 10A and 10B the quantity $\hat{q}/\hat{q}_{\rm SYM}$ is depicted as a function of one rotational parameter (a or b), while another rotational parameter varies. We plot this for various values of $T_{\rm H}$. From Fig. 10A we see that the jet-quenching parameter in the Kerr-AdS$_5$ black hole is larger than that one in the AdS black hole with a planar horizon. It also can be found from Fig. 10A that $\hat{q}$ in Kerr-AdS$_5$ with a fixed b decreases as the parameter a increases. Fig. 10B shows that the dependence of $\hat{q}/\hat{q}_{\rm SYM}$ on the rotational parameter b is nonmonotonic. For some fixed a the quantity $\hat{q}/\hat{q}_{\rm SYM}$ increases as b increases reaching its maximal value and then decreases. This is related to the definition of the "light cone" coordinates (4.20), which yields the emphasis of the parameter a.

It is interesting to compare $\hat{q}$ in Kerr-AdS$_5$ with the jet-quenching parameter in other holographic backgrounds with the rotation. For this we focus on the rotating D-instanton background from [51]. The rotating D-instanton background is characterized by the angular velocity ω and the instanton density q. In Fig. 11 we show the ratio $\hat{q}/\hat{q}_D$ as a function of $T_{\rm H}$, where $\hat{q}$ is the jet-quenching parameter in the Kerr-AdS$_5$ black hole and $\hat{q}_D$ is the jet-quenching parameter in the D-instanton background. We plot $\hat{q}/\hat{q}_D$ in terms of $T_{\rm H}$ for different values of the angular velocity ω and the rotational parameters a and b. From Fig. 11 we observe that for all ω, a, and b, the ratio $\hat{q}/\hat{q}_D$ turns to have a common form; it increases up to some $T_{\rm H}$, and then takes a constant value. Thus, one can conclude that both jet-quenching parameters $\hat{q}$ and $\hat{q}_D$ have the same behavior at high temperatures.

We also present $\hat{q}/\hat{q}_D$ in terms of $T_{\rm H}$, where $\hat{q}$ is taken for the AdS black brane (black dashed line) and the Schwarzschild-AdS$_5$ background (black solid curve), in these cases we set $\omega=0$ for the D-instanton angular velocity. Note that the values of the D-instanton density q are taken in terms of ℓ. In fact, we change q in Fig. 11 from 0 to ℓ^4; however, the dependence of $\hat{q}/\hat{q}_D$ on q is almost negligible. We see that the ratio $\hat{q}/\hat{q}_D$ has a similar

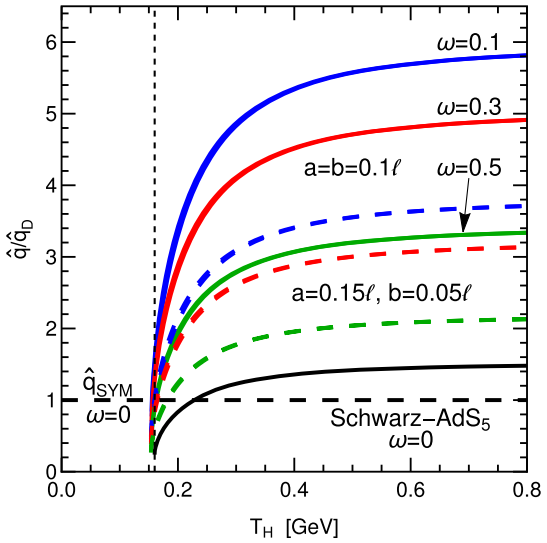

FIG. 11. $\hat{q}/\hat{q}_D$ as a function of $T_{\rm H}$ for various values of the angular velocity of the D-instanton $\omega = 0.1$, 0.3, 0.5 and fixed parameters a and b of Kerr-AdS$_5$; $a = b = 0.1\ell$ (solid) and $a = 0.15\ell$, $b = 0.05\ell$ (dashed). The cases of $\hat{q}/\hat{q}_D$, where $\hat{q}$ corresponds to the AdS-Schwarzschild and AdS black brane are shown by black solid curve and dashed line, correspondingly ($\omega = 0$).

dependence on T_H for both the Kerr-AdS$_5$ and the rotating D-instanton background.

V. CONCLUSIONS AND DISCUSSION

In this paper, we have investigated holographic Wilson loops in the Schwarzschild-AdS$_5$ and Kerr-AdS$_5$ black holes. The both backgrounds have the conformal boundary $R \times \mathbb{S}^3$ and are holographically dual to the nonrotating and rotating $\mathcal{N} = 4$ SYM quark-gluon plasma, correspondingly. In particular, we have calculated the temporal and lightlike Wilson loops in the Schwarzschild-AdS$_5$ and Kerr-AdS$_5$ backgrounds.

From the holographic temporal Wilson loops we have found the quark-antiquark potentials. We have shown that the expressions for the potentials in both backgrounds contain the linear and Coulomb-like terms. At temperatures above the critical one ($T_{\rm H} \geq 0.17$ GeV) we have observed the Coulomb-like behavior (see Figs. 4A, 7A). We have estimated the coefficients of the Coulomb terms both in the Schwarzschild-AdS$_5$ and Kerr-AdS$_5$ backgrounds from fitting of $V_{q\bar{q}}$. For the nonrotating case ($a = b = 0$) we have seen that the distance between quark-antiquark pair can be decreased either by increasing the temperature $T_{\rm H}$ or reducing the angle θ, see Fig. 4A. The same dependence is inherited for the nonzero rotating parameters (see Fig. 6). Note that a similar deformation of the string profile was also observed in [65] for rotating mesons in a static background. We have seen that the rotation increases the values of the quark-antiquark potential $V_{q\bar{q}}$ compared to the Schwarzschild-AdS$_5$ case at the same interquark distance. At high temperatures ($T_{\rm H} = 0.30$ GeV) we have observed that $V_{q\bar{q}}$ in the Kerr-AdS$_5$ background becomes closer to $V_{q\bar{q}}$ in the Schwarzschild-AdS$_5$ black hole (Fig. 7A) at least for certain values of the angle θ (Θ).

Considering the holographic lightlike Wilson loops, we have calculated the jet-quenching parameters $\hat{q}$. For the Schwarzschild-AdS$_5$ black hole we have found that the analytic expression for $\hat{q}$ at high temperatures and $\theta \sim 0$ has a cubic dependence on $T_{\rm H}$, which is similar to that one in the AdS black brane (with a planar horizon) [54]. We have also observed this from the dependence of $\hat{q}/T_H^3$ on $T_{\rm H}/T_{\rm H}^{\rm min}(0,0)$ (see Fig. 8B). As we have seen for $V_{q\bar{q}}$, the value of the jet-quenching parameter $\hat{q}$ also depends on θ. For example, one can obtain a value of $\hat{q}$ at $\theta < \pi/9$, which is smaller than in the AdS black brane.

In the case of Kerr-AdS$_5$ we have found that the jet-quenching parameter increases with the rotation, see Fig. 9A. However, at high temperatures we still have the dependence $\hat{q} \sim \kappa_{\rm rot} T_{\rm H}^3$ with $\kappa_{\rm rot}$ defined by values of a and b. Thus, the cubic dependence of $\hat{q}$ on $T_{\rm H}$ takes place at high temperatures for the rotating and nonrotating cases. In both cases, we have observed a strong dependence on the angle θ (or Θ), which is related to the geometries. Remarkably, in [51] it was found the jet-quenching parameter in the rotating case (the rotating D-instanton background) also takes larger values.

An interesting future direction could be the generalization to a charged Kerr-AdS$_5$ background [66], which corresponds to the case with a nonzero chemical potential. Another interesting problem would be a study of spacial Wilson loops in the Kerr-AdS$_5$ and the Kerr-Newmann-AdS$_5$ black holes and comparing the results with the lattice results for the rotating quark-gluon plasma [43,44]. It would be useful to consider holographic probes moving along a circle in the rotating QGP as was discussed for nonrotating black branes in [67,68].

ACKNOWLEDGMENTS

We are grateful to Irina Aref'eva, Eric Gourgoulhon, Yury Ivanov, Timofey Rusalev and Oleg Teryaev for the valuable discussions. We thank Olesya Geytota for the participation at early stages of the project. We also thank Dimitrios Giataganas and Kazem Bitaghsir Fadafan for the correspondence and useful comments. The present paper were written with the support of the Russian Science Foundation Grant No 22-72-10122.

[1] F. Becattini, V. Piccinini, and J. Rizzo, Angular momentum conservation in heavy ion collisions at very high energy, Phys. Rev. C **77**, 024906 (2008).

[2] Yin Jiang, Zi-Wei Lin, and Jinfeng Liao, Rotating quark-gluon plasma in relativistic heavy ion collisions, Phys. Rev. C **94**, 044910 (2016).

[3] M. I. Baznat, K. K. Gudima, A. S. Sorin, and O. V. Teryaev, Femto-vortex sheets and hyperon polarization in Heavy-Ion Collisions, Phys. Rev. C **93**, 031902 (2016).

[4] Yu. B. Ivanov and A. A. Soldatov, Correlation between global polarization, angular momentum, and flow in heavy-ion collisions, Phys. Rev. C **102**, 024916 (2020).

[5] N. S. Tsegelnik, E. E. Kolomeitsev, and V. Voronyuk, Helicity and vorticity in heavy-ion collisions at energies available at the JINR Nuclotron-based Ion Collider facility, Phys. Rev. C **107**, 034906 (2023).

[6] D. E. Kharzeev, J. Liao, S. A. Voloshin, and G. Wang, Chiral magnetic and vortical effects in high-energy nuclear collisions, A status report, Prog. Part. Nucl. Phys. **88**, 1 (2016).

[7] F. Becattini, V. Chandra, L. Del Zanna, and E. Grossi, Relativistic distribution function for particles with spin at local thermodynamical equilibrium, Ann. Phys. (Amsterdam) **338**, 32 (2013).

[8] F. Becattini and M. A. Lisa, Polarization and vorticity in the quark-gluon plasma, Annu. Rev. Nucl. Part. Sci. **70**, 395423 (2020).

[9] B. I. Abelev *et al.* (STAR Collaboration), Global polarization measurement in Au + Au collisions Phys. Rev. C **76**, 024915 (2007); **95**, 039906(E) (2017).

[10] L. Adamczyk *et al.* (STAR Collaboration), Global Λ hyperon polarization in nuclear collisions: Evidence for the most vortical fluid, Nature (London) **548**, 62 (2017).

[11] H. Petersen, The fastest-rotating fluid, Nature (London) **548**, 34 (2017).

[12] K. Adcox *et al.* (PHENIX Collaboration), Formation of dense partonic matter in relativistic nucleus-nucleus collisions at RHIC: Experimental evaluation by the PHENIX collaboration, Nucl. Phys. **A757**, 184 (2005).

[13] I. Arsene *et al.* (BRAHMS Collaboration), Quark–gluon plasma and color glass condensate at RHIC? The perspective from the BRAHMS experiment, Nucl. Phys. **A757**, 1 (2005).

[14] B. B. Back *et al.*, The PHOBOS perspective on discoveries at RHIC, Nucl. Phys. **A757**, 28 (2005).

[15] J. Adams *et al.* (STAR Collaboration), Experimental and theoretical challenges in the search for the quark–gluon plasma: The STAR Collaboration's critical assessment of the evidence from RHIC collisions, Nucl. Phys. **A757**, 102 (2005).

[16] J. Casalderrey-Solana, H. Liu, D. Mateos, K. Rajagopal, and U. A. Wiedemann, *Gauge/String Duality, Hot QCD and Heavy Ion Collisions* (Cambridge University Press, Cambridge, England, 2014), 10.1017/CBO9781139136747.

[17] I. Ya. Aref'eva, Holographic approach to quark-gluon plasma in heavy ion collisions, Phys. Usp. **57**, 527 (2014).

[18] O. DeWolfe, S. S. Gubser, C. Rosen, and D. Teaney, Heavy ions and string theory, Prog. Part. Nucl. Phys. **75**, 86 (2014).

[19] A. Bazavov *et al.* (HotQCD Collaboration), Equation of state in (2+1)-flavor QCD, Phys. Rev. D **90**, 094503 (2014).

[20] S. J. Rey and J. T. Yee, Macroscopic strings as heavy quarks in large N gauge theory and anti-de Sitter supergravity, Eur. Phys. J. C **22**, 379 (2001).

[21] J. M. Maldacena, Wilson Loops in Large N Field Theories, Phys. Rev. Lett. **80**, 4859 (1998).

[22] S. J. Rey, S. Theisen, and J. T. Yee, Wilson-Polyakov loop at finite temperature in large N gauge theory and anti-de Sitter supergravity, Nucl. Phys. **B527**, 171 (1998).

[23] A. Brandhuber, N. Itzhaki, J. Sonnenschein, and S. Yankielowicz, Wilson loops in the large N limit at finite temperature, Phys. Lett. B **434**, 36 (1998).

[24] A. Brandhuber and K. Sfetsos, Wilson loops from multicenter and rotating branes, mass gaps and phase structure in gauge theories, Adv. Theor. Math. Phys. **3**, 851 (1999).

[25] B. Sundborg, The Hagedorn transition, deconfinement and $N = 4$ SYM theory, Nucl. Phys. **B573**, 349 (2000).

[26] M. Spradlin and A. Volovich, A pendant for polya: The one-loop partition function of $N = 4$ SYM on $R \times S^3$, Nucl. Phys. **B711**, 199 (2005).

[27] T. Harmark and M. Wilhelm, Hagedorn Temperature of AdS_5/CFT_4 via Integrability, Phys. Rev. Lett. **120**, 071605 (2018).

[28] E. Witten, Anti-de Sitter space, thermal phase transition, and confinement in gauge theories, Adv. Theor. Math. Phys. **2**, 505 (1998).

[29] D. Marolf, M. Rangamani, and T. Wiseman, Holographic thermal field theory on curved spacetimes, Classical Quantum Gravity **31**, 063001 (2014).

[30] S. Bhattacharyya, S. Lahiri, R. Loganayagam, and S. Minwalla, Large rotating AdS black holes from fluid mechanics, J. High Energy Phys. 09 (2008) 054.

[31] S. Bhattacharyya, R. Loganayagam, I. Mandal, S. Minwalla, and A. Sharma, Conformal nonlinear fluid dynamics from gravity in arbitrary dimensions, J. High Energy Phys. 12 (2008) 116.

[32] B. McInnes, Applied holography of the AdS_5-Kerr spacetime, Int. J. Mod. Phys. A **34**, 1950138 (2019).

[33] A. Nata Atmaja and K. Schalm, Anisotropic drag force from 4D Kerr-AdS black holes, J. High Energy Phys. 04 (2011) 070.

[34] S. W. Hawking, C. J. Hunter, and M. Taylor-Robinson, Rotation and the AdS/CFT correspondence, Phys. Rev. D **59**, 064005 (1999).

[35] S. W. Hawking and H. S. Reall, Charged and rotating AdS black holes and their CFT duals, Phys. Rev. D **61**, 024014 (2000).

[36] G. W. Gibbons, M. J. Perry, and C. N. Pope, The first law of thermodynamics for Kerr-anti-de Sitter black holes, Classical Quantum Gravity **22**, 1503 (2005).

[37] I. Y. Aref'eva, A. A. Golubtsova, and E. Gourgoulhon, Holographic drag force in 5d Kerr-AdS black hole, J. High Energy Phys. 04 (2021) 169.

[38] X. Chen, L. Zhang, D. Li, D. Hou, and M. Huang, Gluodynamics and deconfinement phase transition under rotation from holography, J. High Energy Phys. 07 (2021) 132.

[39] N. R. F. Braga, L. F. Faulhaber, and O. C. Junqueira, Confinement-deconfinement temperature for a rotating quark-gluon plasma, Phys. Rev. D **105**, 106003 (2022).

[40] Y. Jiang and J. Liao, Pairing Phase Transitions of Matter Under Rotation, Phys. Rev. Lett. **117**, 192302 (2016).
[41] M. N. Chernodub, Inhomogeneous confining-deconfining phases in rotating plasmas, Phys. Rev. D **103**, 054027 (2021).
[42] Y. Fujimoto, K. Fukushima, and Y. Hidaka, Deconfining phase boundary of rapidly rotating hot and dense matter and analysis of moment of inertia, Phys. Lett. B **816**, 136184 (2021).
[43] V. V. Braguta, A. Y. Kotov, D. D. Kuznedelev, and A. A. Roenko, Study of the confinement/deconfinement phase transition in rotating lattice su(3) gluodynamics, JETP Lett. **112**, 1 (2020).
[44] V. V. Braguta, A. Yu. Kotov, D. D. Kuznedelev, and A. A. Roenko, Influence of relativistic rotation on the confinement/deconfinement transition in gluodynamics, Phys. Rev. D **103**, 094515 (2021).
[45] H. Bantilan, T. Ishii, and P. Romatschke, Holographic heavy-ion collisions: Analytic solutions with longitudinal flow, elliptic flow and vorticity, Phys. Lett. B **785**, 201 (2018).
[46] M. Garbiso and M. Kaminski, Hydrodynamics of simply spinning black holes & hydrodynamics for spinning quantum fluids, J. High Energy Phys. 12 (2020) 112.
[47] J. Barragán Amado, B. Carneiro da Cunha, and E. Pallante, Remarks on holographic models of the Kerr-AdS$_5$ geometry, J. High Energy Phys. 05 (2021) 251.
[48] O. V. Geytota, A. A. Golubtsova, H. Dimov, V. H. Nguyen, and R. C. Rashkov, Circular strings in Kerr-AdS$_5$ black holes, Gen. Relativ. Gravit. **55**, 29 (2023).
[49] I. Aref'eva, A. Golubtsova, and E. Gourgoulhon, On the drag force of a heavy quark via 5d Kerr-AdS background, Phys. Part. Nucl. **51**, 535 (2020).
[50] A. A. Golubtsova, E. Gourgoulhon, and M. K. Usova, Heavy quarks in rotating plasma via holography, Nucl. Phys. **B979**, 115786 (2022).
[51] J. X. Chen and D. F. Hou, Heavy quark potential and jet quenching parameter in a rotating D-instanton background, arXiv:2202.00888.
[52] M. Gyulassy and M. Plümer, Jet quenching in dense matter, Phys. Lett. B **243**, 432 (1990).
[53] R. Baier, D. Schiff, and B. G. Zakharov, Energy loss in perturbative QCD, Annu. Rev. Nucl. Part. Sci. **50**, 37 (2000).
[54] H. Liu, K. Rajagopal, and U. A. Wiedemann, Calculating the Jet Quenching Parameter from AdS/CFT, Phys. Rev. Lett. **97**, 182301 (2006).
[55] H. Liu, K. Rajagopal, and U. A. Wiedemann, Wilson loops in heavy ion collisions and their calculation in AdS/CFT, J. High Energy Phys. 03 (2007) 066.
[56] D. Giataganas, Probing strongly coupled anisotropic plasma, J. High Energy Phys. 07 (2012) 031.
[57] K. Rajagopal, A. V. Sadofyev, and W. van der Schee, Evolution of the Jet Opening Angle Distribution in Holographic Plasma, Phys. Rev. Lett. **116**, 211603 (2016).
[58] J. Brewer, A. Sadofyev, and W. van der Schee, Jet shape modifications in holographic dijet systems, Phys. Lett. B **820**, 136492 (2021).
[59] E. Eichten, K. Gottfried, T. Kinoshita, J. Kogut, K. D. Lane, and T.-M. Yan, Spectrum of Charmed Quark-Antiquark Bound States, Phys. Rev. Lett. **36**, 1276 (1976).
[60] E. Eichten, K. Gottfried, T. Kinoshita, K. D. Lane, and T.-M. Yan, Charmonium: The model, Phys. Rev. D **17**, 3090 (1978); **21**, 313(E) (1980).
[61] S. J. Sin and I. Zahed, Holography of radiation and jet quenching, Phys. Lett. B **608**, 265 (2005).
[62] A. Mocsy and P. Petreczky, Can quarkonia survive deconfinement?, Phys. Rev. D **77**, 014501 (2008).
[63] A. Dumitru, Y. Guo, and M. Strickland, The heavy-quark potential in an anisotropic (viscous) plasma, Phys. Lett. B **662**, 37 (2008).
[64] M. Cvetic, P. Gao, and J. Simon, Supersymmetric Kerr-Anti-de Sitter solutions, Phys. Rev. D **72**, 021701 (2005).
[65] V. Giantsos and D. Giataganas, Holographic nonlocal rotating observables and their renormalization, Phys. Rev. D **106**, 126012 (2022).
[66] M. Cvetic, H. Lu, and C. Pope, Charged Kerr-de Sitter black holes in five dimensions, Phys. Lett. B **598**, 273 (2004).
[67] K. Bitaghsir Fadafan, H. Liu, K. Rajagopal, and U. A. Wiedemann, Stirring strongly coupled plasma, Eur. Phys. J. C **61**, 553 (2009).
[68] M. Atashi and K. Bitaghsir Fadafan, Spiraling string in Gauss–Bonnet geometry, Phys. Lett. B **800**, 135090 (2020).